nature cell biology

DAF-16 employs the chromatin remodeller SWI/SNF to promote stress resistance and longevity

Christian G. Riedel[1,2,6], Robert H. Dowen[1,2], Guinevere F. Lourenco[1,2], Natalia V. Kirienko[1,2], Thomas Heimbucher[3], Jason A. West[1,2], Sarah K. Bowman[1,2], Robert E. Kingston[1,2], Andrew Dillin[3], John M. Asara[4,5] and Gary Ruvkun[1,2,7]

Organisms are constantly challenged by stresses and privations and require adaptive responses for their survival. The forkhead box O (FOXO) transcription factor DAF-16 (hereafter referred to as DAF-16/FOXO) is a central nexus in these responses, but despite its importance little is known about how it regulates its target genes. Proteomic identification of DAF-16/FOXO-binding partners in *Caenorhabditis elegans* and their subsequent functional evaluation by RNA interference revealed several candidate DAF-16/FOXO cofactors, most notably the chromatin remodeller SWI/SNF. DAF-16/FOXO and SWI/SNF form a complex and globally co-localize at DAF-16/FOXO target promoters. We show that specifically for gene activation, DAF-16/FOXO depends on SWI/SNF, facilitating SWI/SNF recruitment to target promoters, to activate transcription by presumed remodelling of local chromatin. For the animal, this translates into an essential role for SWI/SNF in DAF-16/FOXO-mediated processes, in particular dauer formation, stress resistance and the promotion of longevity. Thus, we give insight into the mechanisms of DAF-16/FOXO-mediated transcriptional regulation and establish a critical link between ATP-dependent chromatin remodelling and lifespan regulation.

The ability to adapt to stresses and privations is crucial for the survival and thus the longevity of any species. Sophisticated mechanisms are in place to perceive such dire conditions and relay them into the appropriate responses, that is, cytoprotective and homeostatic measures and sometimes even a reversible cessation of development or reproduction[1]. A core pathway for these responses in animals is the environmentally responsive insulin-like signalling pathway with its conserved downstream component, the forkhead transcription factor DAF-16/FOXO (ref. 2). In the presence of ample food and optimal conditions, high insulin-like signalling inactivates DAF-16/FOXO through AKT kinase-mediated phosphorylation, causing cytoplasmic sequestration of DAF-16/FOXO by 14-3-3 proteins. Conversely, under dire conditions, cues that reduce insulin-like signalling and thus allow for reversal of DAF-16/FOXO phosphorylation enable DAF-16/FOXO to translocate to the nucleus, where it engages in transcriptional regulation. Several hundred DAF-16/FOXO target genes have been identified, and it is their concerted action that confers a wide range of beneficial effects on the organism—most notably stress resistance and longevity, but also metabolic responses, stem cell maintenance and tumour suppression[3,4]. Although many studies have explored the signalling pathways leading to DAF-16/FOXO activation, little is known about the mechanisms or cofactors by which DAF-16/FOXO regulates its target genes.

RESULTS

Identification of candidate DAF-16/FOXO cofactors

To address this problem we used the nematode *Caenorhabditis elegans*, a model system that has been instrumental in dissecting the functions of DAF-16/FOXO, mostly owing to its amenability for genetic manipulation and its compatibility with high-throughput screening approaches for developmental arrest, stress resistance and lifespan phenotypes. We biochemically characterized DAF-16/FOXO by size-exclusion chromatography of whole *C. elegans* lysates, which revealed that a significant amount of DAF-16/FOXO partitions to high-molecular-weight fractions (Fig. 1a). Activation of DAF-16/FOXO in a *daf-2* (insulin or IGF receptor) mutant background increased the partitioning of DAF-16/FOXO to these fractions (Fig. 1a), suggesting that DAF-16/FOXO activity involves and maybe even requires binding to other proteins, that is, cofactors. Hence, we conducted a screen to identify cofactors of DAF-16/FOXO, in which we combined proteomic identification of DAF-16/FOXO-binding partners with high-throughput functional assays using RNA interference (RNAi;

[1]Department of Molecular Biology, Massachusetts General Hospital, Boston, Massachusetts 02114, USA. [2]Department of Genetics, Harvard Medical School, Boston, Massachusetts 02114, USA. [3]Molecular and Cell Biology Laboratory, The Salk Institute for Biological Studies, La Jolla, California 92037, USA. [4]Division of Signal Transduction, Beth Israel Deaconess Medical Center, Boston, Massachusetts 02115, USA. [5]Department of Medicine, Harvard Medical School, Boston, Massachusetts 02115, USA. [6]Present address: European Research Institute for the Biology of Ageing, University Medical Center Groningen, 9713 AV Groningen, The Netherlands. [7]Correspondence should be addressed to G.R. (e-mail: ruvkun@molbio.mgh.harvard.edu)

Received 23 October 2012; accepted 28 February 2013; published online 21 April 2013; DOI: 10.1038/ncb2720

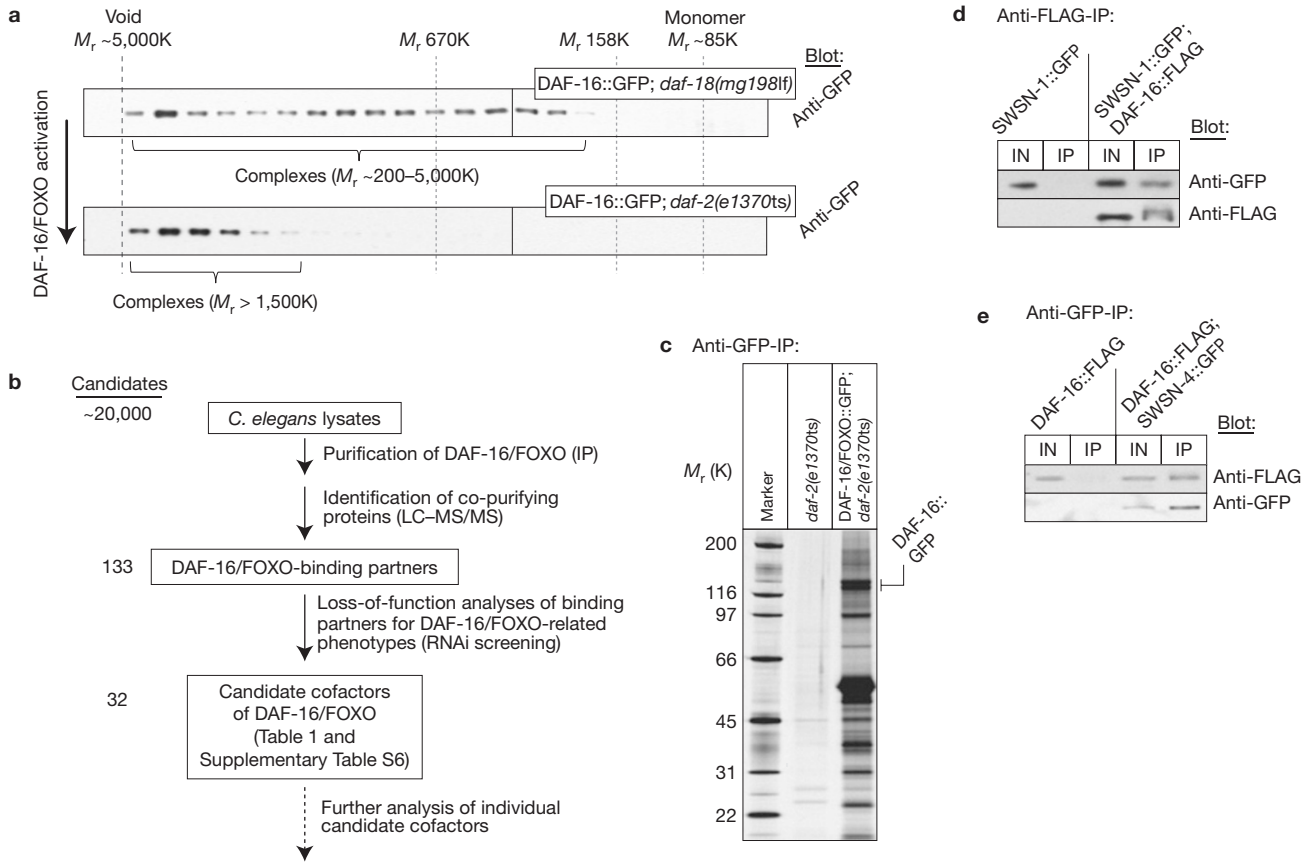

Figure 1 DAF-16/FOXO binds to the chromatin remodeller SWI/SNF. (**a**) *C. elegans* strains yielding inactive cytoplasmic DAF-16/FOXO (*daf-18(mg198*lf)/PTEN mutant) or active nuclear DAF-16/FOXO (*daf-2(e1370*ts)/insulin–IGF receptor mutant) were shifted for 20 h to restrictive temperature, lysed and lysates separated on a Superose 6 size-exclusion column. Fractions were analysed by SDS–PAGE and western blotting. (**b**) Schematic of the screen for DAF-16/FOXO cofactors. IP, immunoprecipitation. LC–MS/MS, liquid chromatography followed by tandem mass spectrometry. (**c**) SDS–PAGE and silver stain analysis of large-scale anti-GFP immunoprecipitations from indicated strains. (**d**,**e**) Confirmatory co-immunoprecipitations. DAF-16/FOXO::FLAG (**d**) or SWSN-4::GFP (**e**) was immunoprecipitated from whole-worm lysates of the indicated strains. Benzonase (50 U ml^{-1}) was added to eliminate DNA- or RNA-mediated interactions. Samples were analysed by SDS–PAGE and western blotting. For some inputs (IN), only fractions were loaded: 2% for SWSN-1::GFP (**d**), 2% for DAF-16::FLAG (**e**) and 20% for SWSN-4::GFP (**e**). Uncropped images of blots are shown in Supplementary Fig. S8.

Fig. 1b). Epitope-tagged DAF-16/FOXO was immunoprecipitated in different states of activation, using three different *C. elegans* genetic backgrounds: wild-type (DAF-16 partially active), *daf-2(e1370*ts) at restrictive temperature (insulin/IGF receptor mutant; DAF-16 fully active) or *daf-18(mg198*lf) (PTEN mutant, causing constitutively high PIP_3 signalling that, in turn, constitutively activates the AKT kinases that phosphorylate and inactivate DAF-16/FOXO; DAF-16 inactive). Proteins that specifically co-purified with DAF-16/FOXO were identified by liquid chromatography followed by tandem mass spectrometry (see also Fig. 1c). In addition to previously known DAF-16/FOXO-binding partners (that is, the 14-3-3 proteins FTT-2 and PAR-5 (ref. 5)), we identified 131 new binding partners of DAF-16/FOXO, most of which were enriched in purifications of active DAF-16/FOXO (Supplementary Table S1).

To identify potential DAF-16/FOXO cofactors amongst these binding partners, we silenced their expression by RNAi and examined a range of ageing and gene expression phenotypes expected from altered DAF-16/FOXO activity: to identify cofactors required for DAF-16/FOXO activity, we tested each gene inactivation for impaired DAF-16/FOXO-induced lifespan extension or an inability to upregulate the DAF-16/FOXO-activated gene *sod-3* in *daf-2* mutant animals (Table 1 and Supplementary Tables S2 and S3). To identify interacting proteins that antagonize DAF-16/FOXO activity, we tested each gene inactivation for an extension of lifespan or inappropriate induction of *sod-3* in otherwise wild-type animals (Supplementary Tables S4–S6). Out of 72 DAF-16/FOXO-binding partners tested, inactivation of the genes encoding 32 of them caused significant phenotypes in at least one of the assays. Thus, they were considered candidate cofactors of DAF-16/FOXO (Table 1 and Supplementary Table S6). Comparison of the frequency of phenotypes in Supplementary Table S2 with a similar genome-wide survey[6] indicated that our list of binding partners was more than 20-fold enriched for proteins involved in DAF-16/FOXO function, underscoring the utility of this co-purification approach. Many of the 32 candidate cofactors act in the regulation of chromatin and transcription (for example, SWSN-1, SWSN-3, BAF-1, ELB-1, DCP-66, DPY-30, ZFP-1 and MRG-1) or protein folding and homeostasis (for example, RPN-9, RPN-12, CCT-8, PFD-6 and PFD-2; Table 1; Supplementary Table S6), both of which are

Table 1 Short-list of candidate DAF-16/FOXO cofactors required for DAF-16/FOXO function.

	Gene targeted by RNAi*	Public name	Annotation	M_r(K)	Spectral counts (MS/MS)	Functional evaluation (Supplementary Tables S2 and S3)‡ *daf-2(e1370ts)*-specific lifespan change (%)	Functional evaluation (Supplementary Tables S2 and S3)‡ Expression of *Psod-3::GFP* in *daf-2(e1370ts)* (a.u.)†
	Empty vector	Control	–	–	–	0.0	4.0
	R13H8.1	DAF-16	Forkhead transcription factor	60	221	−40.4	1.0
→	Y113G7B.23	SWSN-1	SWI/SNF subunit (BAF155/170)	85	17	−48.2	1.7
	T06D8.8	RPN-9	Proteasome subunit	44	3	−46.6	2.8
	W07G4.4	LAP-2	Leucine aminopeptidase	56	5	−42.3	4.0
	B0464.7	BAF-1	Chromatin factor	10	7	−36.2	4.0
	C41D11.2	EIF-3.H	Translation initiation factor	41	3	−35.3	n/d
	Y55F3AR.3	CCT-8	Chaperone subunit	60	12	−33.4	2.5
	Y41C4A.10	ELB-1	Transcription elongation factor	13	4	−32.7	4.0
	F21C3.5	PFD-6	Chaperone subunit	15	3	−28.9	4.0
	C18G1.5	HIL-4	Histone H1	26	3	−26.2	4.0
	F26E4.4	F26E4.4	Unknown	44	5	−25.5	4.0
→	Y71H2AM.17	SWSN-3	SWI/SNF subunit (BAF57)	39	10	−24.8	4.0
	H19N07.3	H19N07.3	Unknown	20	7	−24.1	4.0
	Y71F9B.4	SNR-7	Small nuclear RNP	9	3	−22.5	n/d
	R10E4.2	SUP-26	RNA-binding protein	39	3	−21.5	3.8
	Y57G11C.3	Y57G11C.3	6-phosphogluconolactonase	30	8	−21.1	4.0
	C08B11.7	UBH-4	Ubiquitin hydrolase	37	2	−20.9	4.0
	C26C6.5	DCP-66	NuRD subunit	77	5	−18.1	1.0
	H20J04.8	MOG-2	Small nuclear RNP	29	2	−17.4	3.2
	H32C10.2	LIN-33	Unknown	27	3	−12.7	3.2
	F17C11.9	EEF-1G	Translation elongation factor	44	3	24.5	3.0

Controls

Intensity of the phenotype

The table was sorted by the intensity of the lifespan phenotypes. Red arrows highlight SWI/SNF subunits. For the full list of functional evaluation data, see Supplementary Tables S2–S6. MS/MS, tandem mass spectrometry. *For *rpn-9, baf-1* and *cct-8* several RNAi clones were tested and the results were averaged for this table. †For a description of the GFP expression scoring scale, see Supplementary Table S3. ‡The intensity of the red colour denotes the intensity of the phenotype.

important for stress response and lifespan regulation[7,8]. Some of the candidate cofactors even emerged from previous ageing-related studies; for example, BAF-1 controls age-dependent muscle integrity[9] and CCT-8 is a component of the lifespan-regulatory cytosolic chaperonin T complex[10].

SWI/SNF binds to and co-localizes with DAF-16/FOXO

Although follow-up of several of these candidate cofactors may yield compelling insight into DAF-16/FOXO mechanism and function, we focused on a candidate with particularly strong phenotypes in both regulation of lifespan and expression of *sod-3*: SWSN-1 (orthologue of human BAF155 and BAF170), a core subunit of the chromatin remodeller SWI/SNF. Two other SWI/SNF subunits, SWSN-3 (orthologue of human BAF57) and SWSN-8 (orthologue of human BAF250 or OSA), were amongst our 32 candidate cofactors or at least emerged from the proteomic analysis (Table 1 and Supplementary Table S1).

SWI/SNF is an essential multi-subunit complex with a relative molecular mass of 1,000,000–2,000,000 that repositions, exchanges or displaces nucleosomes in an ATP-dependent manner[11,12] (Supplementary Fig. S1a,b). The BRG1 or BRM orthologue SWSN-4 provides the complex's catalytic activity and comprises, together with SWSN-1 and SNFC-5 (orthologue of INI1), its core subunits[13]. Other accessory subunits direct the specificity of the complex. In particular, two subclasses of SWI/SNF, BAF and PBAF, which differ by the presence of accessory signature subunits (in particular SWSN-8 and PBRM-1 (orthologue of Polybromo); Supplementary Fig. S1a,b), show distinct functions[14,15]. Although chromatin remodelling is a ubiquitous process, the roles of SWI/SNF are surprisingly confined. For example, in yeast only 6% of all gene expression events depend on SWI/SNF (ref. 16), suggesting that particular mechanisms direct SWI/SNF to specific sites.

In *C. elegans*, studies on SWI/SNF have remained few—mostly focused on its role in asymmetric T-cell division and gonad morphogenesis[15,17]. To explore the relationship between DAF-16/FOXO and SWI/SNF, we first confirmed the interaction between DAF-16/FOXO and SWI/SNF subunits (including its catalytic core SWSN-4) and excluded the possibility of a DNA-mediated interaction by co-immunoprecipitation in the presence of Benzonase, a nuclease that degrades DNA and RNA (Fig. 1d,e). Next we determined in which tissues and subcellular compartments DAF-16/FOXO and SWI/SNF are co-expressed and hence their interaction may occur. Both were expressed globally, including the tissues important for DAF-16/FOXO function (in particular intestine and neurons[17,18]; Supplementary Fig. S1c). Whereas inactive DAF-16/FOXO (for example, in *daf-18(mg198*lf)) is sequestered in the cytoplasm and translocates to the nucleus only on its activation (for example, in *daf-2(e1370*ts)), SWI/SNF subunits resided constitutively in the nucleus[15,17,19] (Supplementary Fig. S1c; data not shown). Consistent

with this observation, mass spectrometric comparison of the DAF-16/FOXO purifications from wild-type, *daf-2(e1370*ts) and *daf-18(mg198*lf) animals revealed a positive correlation between the activation of DAF-16/FOXO and its binding to SWI/SNF (comparison based on spectral counts, Supplementary Table S1). Thus, it seems that DAF-16/FOXO and SWI/SNF encounter each other in most cell types, with their interaction preferentially occurring following DAF-16/FOXO activation and translocation into the nucleus, in particular under low insulin-like signalling conditions.

SWI/SNF is required for DAF-16/FOXO-mediated transcriptional regulation

Next we evaluated the importance of SWI/SNF for DAF-16/FOXO activity. As DAF-16/FOXO exerts its function by transcriptional regulation of target genes, we investigated whether SWI/SNF is required for this regulation to occur. We used transcriptional reporters of two DAF-16/FOXO-regulated genes, *sod-3* and *ins-7*, to examine DAF-16/FOXO-dependent transcriptional activation and repression, respectively[6,20]. Expression of the *Psod-3::GFP* reporter is induced under conditions of low insulin-like signalling, for example, in *daf-2* mutants[18]. Further inactivation by RNAi of DAF-16/FOXO or of the SWI/SNF core subunits SWSN-4 and SWSN-1 and the BAF-subclass signature subunit SWSN-8 suppressed this induction of *Psod-3::GFP* (Fig. 2a,b). Likewise, repression of *Pins-7::ins-7::GFP* was suppressed by RNAi against SWI/SNF subunits, in particular SWSN-4 and SWSN-1 and to a lesser extent SWSN-8, SWSN-3 and SNFC-5 (Fig. 2c,d). It is important to note that in contrast to the BAF-subclass signature subunit SWSN-8, RNAi against the PBAF-subclass signature subunits PBRM-1, TAG-298 (orthologue of BRD7) or SWSN-7 (orthologue of BAF200) (by validated RNAi conditions (Supplementary Fig. S2)) yielded no significant phenotypes in these assays, suggesting that specifically a BAF-like subclass of the SWI/SNF complex mediates DAF-16/FOXO functions.

We then examined whether SWI/SNF is required for the regulation of endogenous DAF-16/FOXO target genes genome-wide. By high-throughput sequencing of messenger RNA (mRNA-seq), we compared gene expression levels between wild-type, *daf-2(e1370*ts), *daf-2(e1370*ts); *daf-16(0)*, and *daf-2(e1370*ts); *swsn-1(os22*ts*)* young adult animals at restrictive temperature. First we investigated whether *daf-16(0)* or *swsn-1(os22*ts*)* could suppress the differential gene expression caused by decreased insulin-like signalling in *daf-2(e1370*ts), which is thought to be entirely mediated by DAF-16/FOXO (ref. 3). As indicated by an extensive reversal of the differential gene expression to wild-type levels (78% of genes activated and 71% of genes repressed in the *daf-2(e1370*ts) mutant), *daf-16(0)* largely suppressed the gene expression changes induced by *daf-2(e1370*ts) (Fig. 3a,b). Likewise, *swsn-1(os22*ts*)* significantly reversed this differential gene expression, although to a lesser extent (42% of genes activated and 32% of genes repressed in the *daf-2(e1370*ts) mutant were reverted; Fig. 3a,b). This could be due to *swsn-1(os22*ts*)* being a non-null and therefore weaker allele than *daf-16(0)*, SWSN-1 being less important, or it acting on only a subset of DAF-16/FOXO target genes. Next we determined the overlap between DAF-16/FOXO- and SWI/SNF-regulated genes. Importantly, although DAF-16/FOXO and SWI/SNF each regulate only a small fraction of the genome (5.9% and 7.5%, respectively), their dependent gene sets showed substantial and significant overlap: of the 656 genes activated and 356 genes repressed by DAF-16/FOXO in *daf-2(e1370*ts) animals, 32% (211) of the activated and 15% (53) of the repressed genes were co-regulated by SWI/SNF (Fig. 3c), suggesting that a large fraction of DAF-16/FOXO-mediated gene regulatory events require SWI/SNF. Gene Ontology term analysis of the co-dependent genes showed significant enrichment for genes involved in ageing, oxidative stress response and organismal defence (Supplementary Table S7). Focusing on DAF-16/FOXO target genes, specifically for genes activated by DAF-16/FOXO we observed a strong positive correlation between the extent of DAF-16/FOXO-mediated activation and the requirement of SWI/SNF for this activation to occur (as indicated by a declining trend line in Fig. 3d, right panel). No such substantial correlation was found for genes non-regulated or repressed by DAF-16/FOXO (Fig. 3d, left and middle panels). Thus, SWI/SNF is required for the regulation of a large subset of DAF-16/FOXO target genes—predominantly those activated by DAF-16/FOXO.

DAF-16/FOXO and SWI/SNF co-localize on chromatin

We then sought the mechanism by which SWI/SNF impacts DAF-16/FOXO-mediated gene regulation. Given that SWI/SNF and activated DAF-16/FOXO are both known to associate with DNA (refs 2,11,12), we determined the genome-wide positioning of DAF-16/FOXO, the SWI/SNF catalytic subunit SWSN-4 and the SWI/SNF core regulatory subunit SWSN-1 in *daf-2(e1370*ts) animals at restrictive temperature using chromatin immunoprecipitation followed by high-throughput sequencing (ChIP-seq). Using strains expressing either DAF-16::GFP, SWSN-4::GFP or SWSN-1::GFP, we identified 1,952 binding sites for DAF-16/FOXO, 3,804 binding sites for SWSN-4 and 5,727 binding sites for SWSN-1. Despite our use of multi-copy transgenes that may be expressed at non-physiological levels, we observed a reassuring enrichment for the canonical DAF-16/FOXO-associated motif TRTTTAC (ref. 3) at DAF-16/FOXO-binding sites. SWSN-4- and SWSN-1-binding sites were likewise enriched for several motifs, although motifs of less defined roles (Supplementary Table S8). Interestingly, not only SWI/SNF- but also DAF-16/FOXO-binding sites shared enrichment for a motif known to associate with Trithorax-like, a protein of *Drosophila melanogaster* that is functionally related to SWI/SNF (ref. 21 and Supplementary Table S8). DAF-16/FOXO-binding sites in *daf-2(e1370*ts) correlated well with DAF-16/FOXO-binding sites previously identified in wild-type animals[4] (Supplementary Fig. S3a). Furthermore, DAF-16/FOXO as well as SWI/SNF-binding sites were mostly located within promoter regions, consistent with these proteins functioning in transcriptional regulation (Fig. 4a). Genes immediately downstream of DAF-16/FOXO-binding sites were strongly enriched for DAF-16/FOXO-activated genes, whereas they were depleted for DAF-16/FOXO-repressed genes (Fig. 4b). Of the directly regulated genes, 87% experienced activation and only 13% repression by DAF-16/FOXO, suggesting that DAF-16/FOXO is predominantly a transcriptional activator.

Given that DAF-16/FOXO and SWI/SNF form a complex (Fig. 1d,e and Supplementary Table S1), we investigated whether they would co-localize also on chromatin. Indeed, SWSN-4 and SWSN-1 were strongly enriched right at the summits of DAF-16/FOXO-binding sites (Fig. 4c,e), supporting the model of DAF-16/FOXO–SWI/SNF interaction. Furthermore, the fact that this co-localization occurred

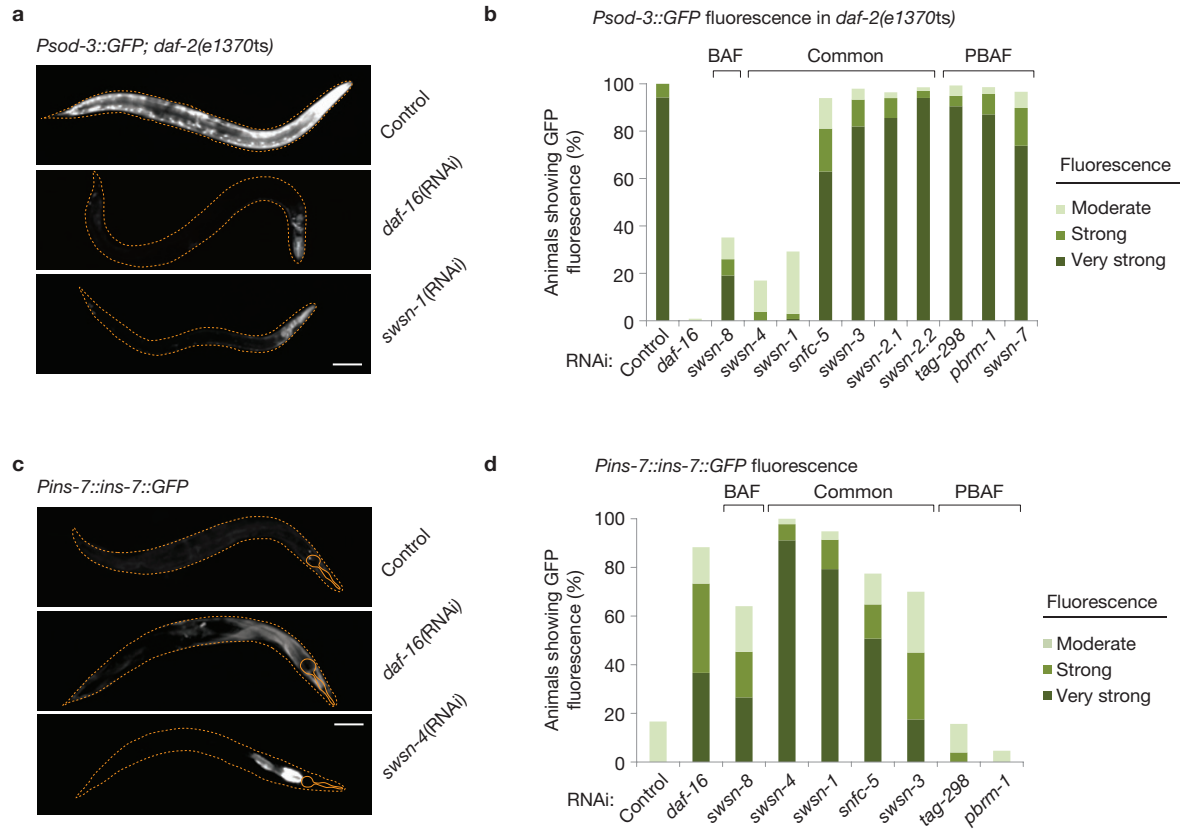

Figure 2 A BAF-like subclass of SWI/SNF is required for regulation of DAF-16/FOXO target genes. (**a**–**d**) *Psod-3::GFP*; *daf-2(e1370*ts) (**a**,**b**) or *Pins-7::ins-7::GFP* (**c**,**d**) animals were grown from the L1 stage on the indicated RNAi bacteria. *daf-2(e1370*ts) was inactivated by a shift to restrictive temperature at the L4 stage. GFP fluorescence intensity was evaluated on day 4 of adulthood ($n = 50$ animals). Representative images are shown (scale bar, 100 μm; **a**,**c**). Common SWI/SNF subunits or ones specific to the subclasses BAF or PBAF are indicated accordingly (**b**,**d**).

not only at some but most DAF-16/FOXO-binding sites (Fig. 4d,e) further supports the intimate connection between DAF-16/FOXO and this cofactor.

DAF-16/FOXO recruits SWI/SNF to directly activated target genes

There is substantial precedence for transcription factors to employ chromatin remodellers as cofactors[12]. In the case of SWI/SNF, some transcription factors recruit it to target promoters to induce local nucleosome repositioning that alters the accessibility of *cis*-regulatory promoter elements to regulate transcription[22]. To determine whether DAF-16/FOXO employs SWI/SNF in a similar manner, we investigated whether their binding to DAF-16/FOXO target promoters depends on each other. Inactivation of SWI/SNF by use of *swsn-1(os22*ts) at restrictive temperature had no effect on DAF-16/FOXO expression, nuclear localization nor its binding to target promoters (Fig. 5a and Supplementary Fig. S3b,c). Next we examined the SWI/SNF catalytic core subunit, SWSN-4. Again, loss of DAF-16/FOXO did not alter SWSN-4 expression levels (Supplementary Fig. S3b), or its nuclear localization (Supplementary Fig. S3c), nor did we observe significant changes in the abundance of SWSN-4 at promoters that were either non-regulated or repressed by DAF-16/FOXO (Fig. 5b). However, specifically at a large fraction of promoters that were directly bound and activated by DAF-16/FOXO (for example, promoters of *sod-3*, *ctl-3* or *hil-1*) we observed a substantial loss of SWSN-4 binding in the absence of DAF-16/FOXO (Fig. 5b,d; Supplementary Fig. S4a). As a further control, we investigated promoters that were activated by DAF-16/FOXO (as judged by mRNA-seq) but were lacking a DAF-16/FOXO-binding site, assuming that these are only indirect targets of DAF-16/FOXO, for example, regulated by transcription factors or other events downstream of DAF-16/FOXO. Here we observed no change in SWSN-4 binding on loss of DAF-16/FOXO, suggesting that SWSN-4 recruitment at directly DAF-16/FOXO-activated promoters is indeed controlled by the physical presence of DAF-16/FOXO and not mere events of transcriptional activation (Fig. 5b). Findings for SWSN-4 were confirmed by analysis of SWSN-1, yielding similar results (Fig. 5c and Supplementary Figs S3b and S4a, data not shown). Results were also confirmed and replicated by conventional ChIP–quantitative PCR (ChIP–qPCR) experiments (Supplementary Fig. S4b). We conclude that DAF-16/FOXO employs SWI/SNF as a cofactor in the manner previously described for other transcription factors, and hence we infer the following model for how DAF-16/FOXO may activate its target genes: DAF-16/FOXO binds promoters in a manner that is independent of SWI/SNF, presumably by directly accessing its target sequences, and at promoters that DAF-16/FOXO directly activates, it aids the recruitment of SWI/SNF, thereby inducing local chromatin remodelling. This remodelling enhances accessibility of activatory *cis*-regulatory promoter elements for binding by downstream

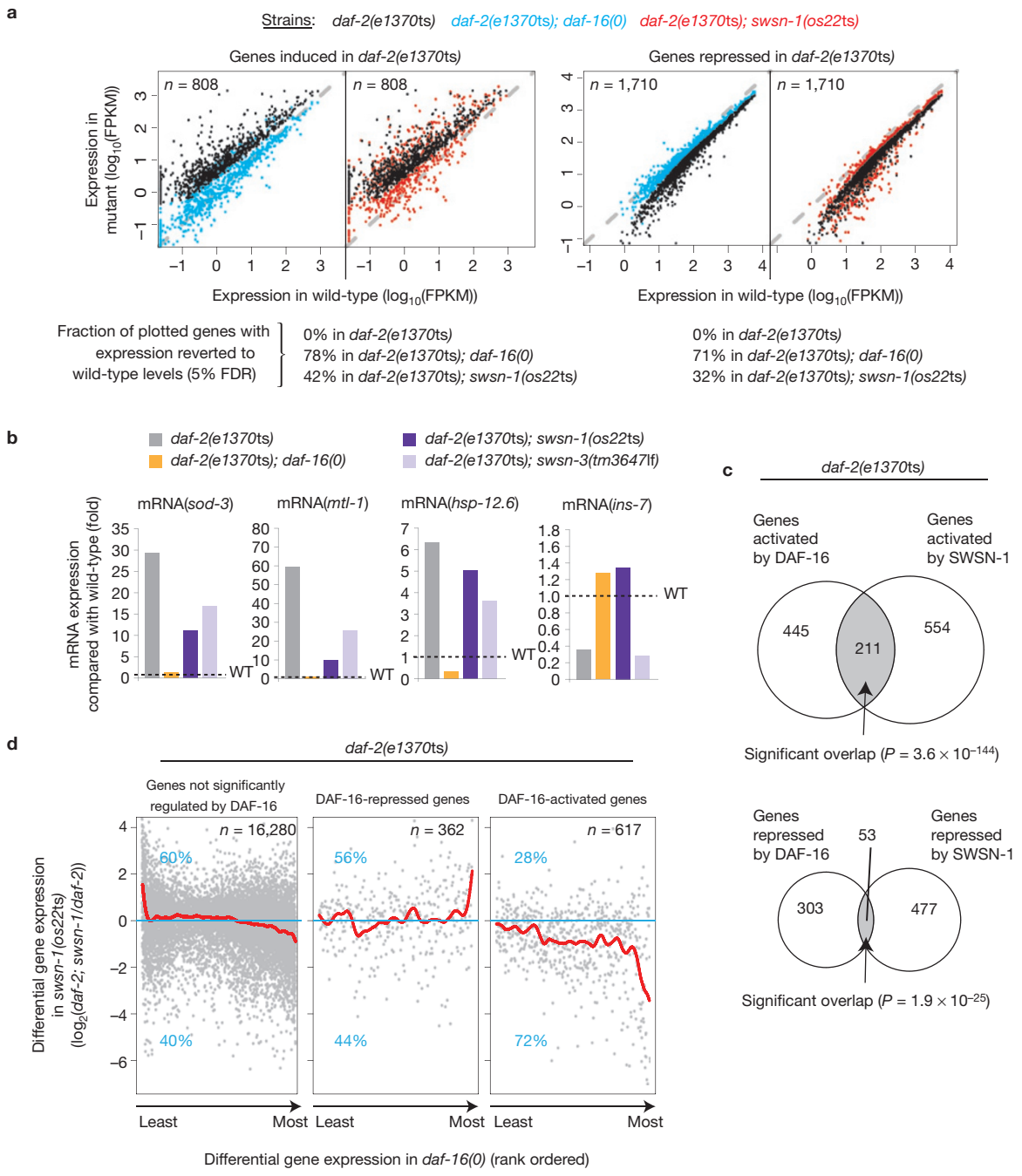

Figure 3 SWI/SNF is required for regulation of a large fraction of DAF-16/FOXO target genes—in particular those activated by DAF-16/FOXO. Wild-type, *daf-2(e1370*ts), *daf-2(e1370*ts); *daf-16(0)*, and *daf-2(e1370*ts); *swsn-1(os22*ts*)* *C. elegans* were grown to the L4 stage, and then shifted to restrictive temperature. After 20 h, genome-wide mRNA expression levels were determined by mRNA-seq. (**a**) Scatter-plots comparing gene expression in wild-type with that of various mutant strains. Only genes either significantly induced by *daf-2(e1370*ts) (left panel) or repressed by *daf-2(e1370*ts) (right panel) are shown. Colours indicate the strains in which the gene expression was analysed. As indicated by reversion of many genes to wild-type expression levels (shift of genes to the plots' indicated diagonals), *daf-16(0)* extensively and *swsn-1(os22*ts*)* partially suppress the gene expression changes of *daf-2(e1370*ts) animals. (**b**) Confirmation of the mRNA-seq data by reverse transcription and qPCR, showing the expression levels of endogenous *sod-3*, *mtl-1*, *hsp-12.6* and *ins-7*. Expression levels shown are relative to wild-type (WT) levels (black dotted lines). Consistent with the mRNA-seq results, *daf-16(0)* tends to fully and mutants in SWI/SNF tend to partially suppress the differential gene expression caused by *daf-2(e1370*ts). (**c**) Significant overlap between genes regulated by DAF-16/FOXO and SWSN-1/BAF155/170 (hypergeometric test). Genes downregulated in either *daf-2(e1370*ts); *daf-16(0)* or *daf-2(e1370*ts); *swsn-1(os22*ts*)* compared with *daf-2(e1370*ts) are shown in the upper diagram; genes upregulated in these comparisons are shown in the lower diagram. (**d**) Correlation between the extent of DAF-16/FOXO- and SWI/SNF-mediated differential gene expression in *daf-2(e1370*ts) animals. Red lines represent trend lines; blue numbers show the fraction of genes that are either up- or downregulated in *swsn-1(os22*ts*)*; *n* denotes the number of DAF-16/FOXO-non-regulated, repressed or activated genes contributing to each of the plots. Specifically for genes activated by DAF-16/FOXO in *daf-2(e1370*ts), the extent of DAF-16/FOXO-mediated activation correlates with an increasing dependence on SWI/SNF, as indicated by the declining trend line in the plot on the right.

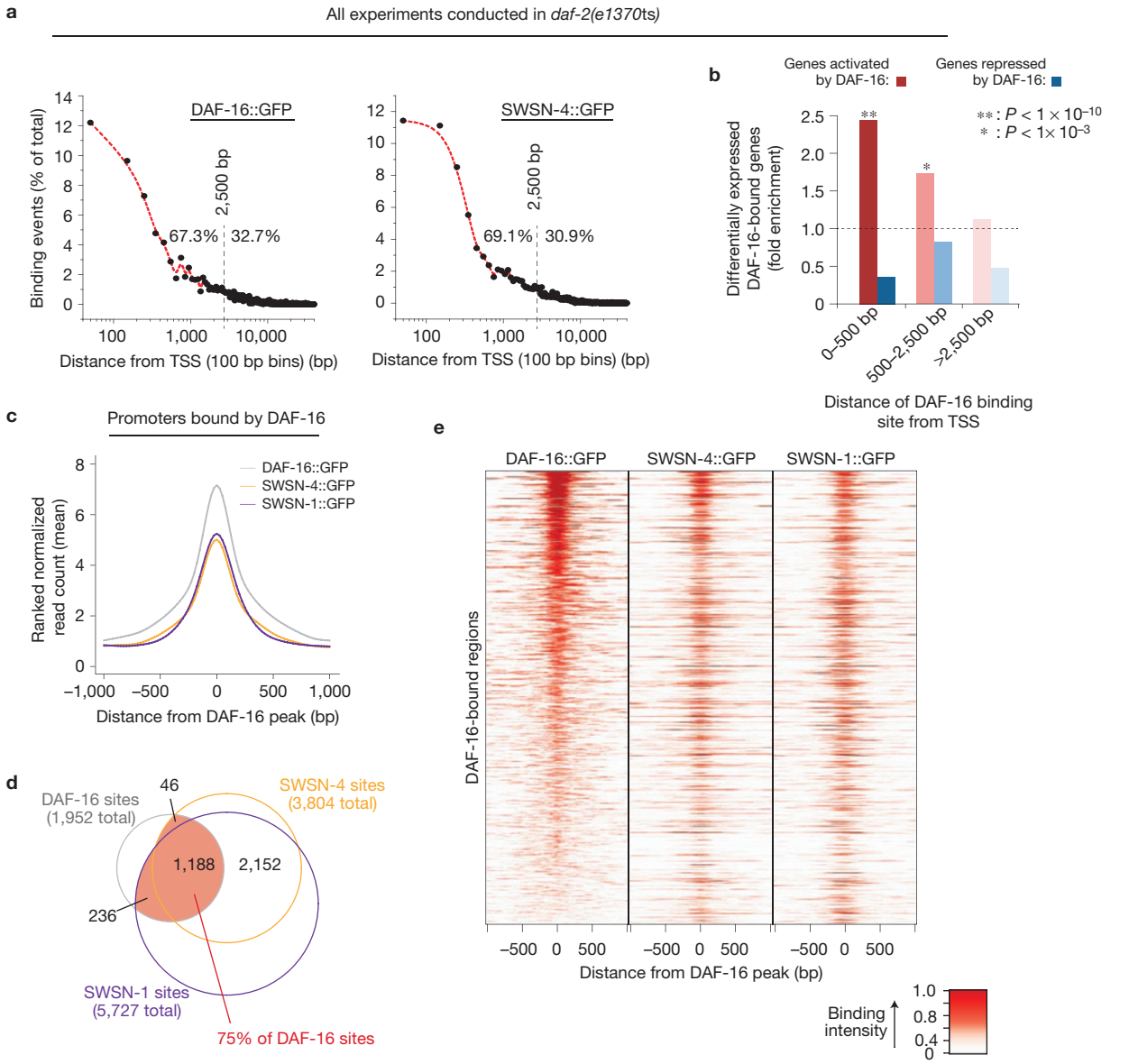

Figure 4 SWI/SNF extensively associates with DAF-16/FOXO-bound promoter regions. *C. elegans* of either *daf-2(e1370*ts); DAF-16::GFP, *daf-2(e1370*ts); SWSN-4::GFP, or *daf-2(e1370*ts); SWSN-1::GFP were grown asynchronously and *e1370ts* was inactivated by a 20 h shift to restrictive temperature. ChIP-seq of GFP-tagged proteins was performed and binding sites were determined. (**a**) Each binding site was associated with its closest transcriptional start site (TSS) and distances were plotted, revealing that DAF-16/FOXO and SWI/SNF are predominantly located within 2.5 kb of a TSS and thus within promoter regions. (**b**) Genes in the vicinity of a DAF-16/FOXO-binding site are strongly enriched for DAF-16/FOXO-activated genes and depleted for DAF-16/FOXO-repressed genes. This effect decays with the distance of the binding site from the TSS. (**c**) DAF-16/FOXO-bound promoter regions are strongly enriched for binding by SWSN-4::GFP and SWSN-1::GFP. Mean read distributions across all DAF-16/FOXO-binding sites are shown for the indicated strains. (**d**) Venn diagram showing the overlap between binding sites for DAF-16/FOXO, SWSN-4 and SWSN-1. The red area highlights DAF-16-binding sites that overlap with any SWI/SNF-binding site. (**e**) Heat-map representation of the data contributing to **c**,**d**, further supporting that SWI/SNF binding occurs at most DAF-16/FOXO-binding sites. The lines of the heat map represent the individual DAF-16/FOXO-bound regions and are sorted by the intensity of DAF-16/FOXO binding.

components (for example, the transcription machinery), thereby resulting in transcriptional activation (Supplementary Fig. S5).

SWI/SNF is required for DAF-16/FOXO-mediated dauer formation

Given our collective evidence that DAF-16/FOXO employs SWI/SNF as a gene-activation-specific cofactor, we then wondered about the importance of this cofactor for the various DAF-16/FOXO-mediated functions in the animal. In *C. elegans*, DAF-16/FOXO is required for entry into the dauer state, a developmental arrest or diapause state that allows for survival in many adverse conditions[23]. We induced this state by inactivating insulin-like signalling and tested whether RNAi against SWI/SNF subunits was able to suppress it. Consistent with SWI/SNF being an important cofactor to DAF-16/FOXO, not only loss

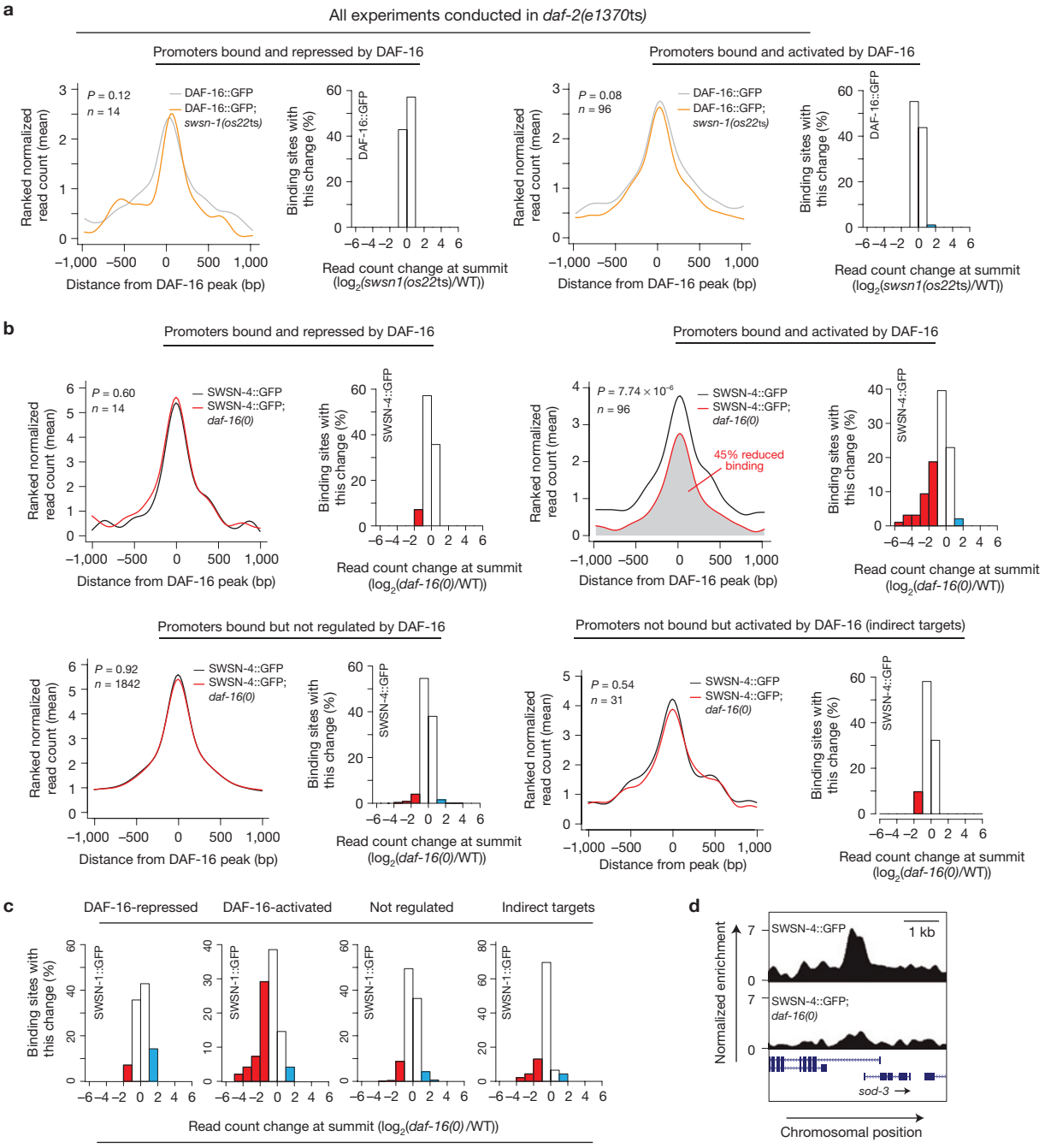

Figure 5 DAF-16/FOXO recruits SWI/SNF specifically to target promoters that are directly activated by DAF-16/FOXO. *C. elegans* of either *daf-2(e1370*ts); DAF-16::GFP, *daf-2(e1370*ts); *swsn-1* (*os22*ts); DAF-16::GFP, *daf-2(e1370*ts); SWSN-4::GFP, *daf-2(e1370*ts); *daf-16(0)*; SWSN-4::GFP, *daf-2(e1370*ts); SWSN-1::GFP, or *daf-2(e1370*ts); *daf-16(0)*; SWSN-1::GFP were grown asynchronously and *e1370*ts and *os22*ts alleles were inactivated by a 20 h shift to restrictive temperature. ChIP-seq of GFP-tagged proteins was performed. (**a**) DAF-16/FOXO binding to promoter regions is not affected by the absence of SWI/SNF. Mean read distributions across different subsets of DAF-16/FOXO target promoters are shown for the indicated strains. *n* denotes the number of promoter regions used in each analysis and *P* values denote the significance of the change in DAF-16/FOXO binding. Corresponding histograms illustrate that hardly any of the promoters underwent a binding change larger than twofold. WT, wild-type. (**b**) Loss of DAF-16/FOXO impairs binding of SWSN-4 specifically to promoters directly bound and activated by DAF-16/FOXO. Mean read distributions across different subsets of DAF-16/FOXO target promoters are shown for the indicated strains. *n* denotes the number of promoter regions used in each analysis and *P* values denote the significance of the change in SWSN-4 binding. Corresponding histograms illustrate the fraction of promoters that underwent a larger than twofold change in SWSN-4 binding (coloured regions). (**c**) Histograms illustrating that loss of DAF-16/FOXO likewise impairs binding of SWSN-1 specifically to promoters directly bound and activated by DAF-16/FOXO. (**d**) Prominent example of *daf-16(0)*-dependent changes in SWSN-4 binding to the *sod-3* promoter (a promoter directly bound and activated by DAF-16/FOXO). ChIP-seq data were normalized, smoothed over 50 bp bins, and then shown in the UCSC genome browser.

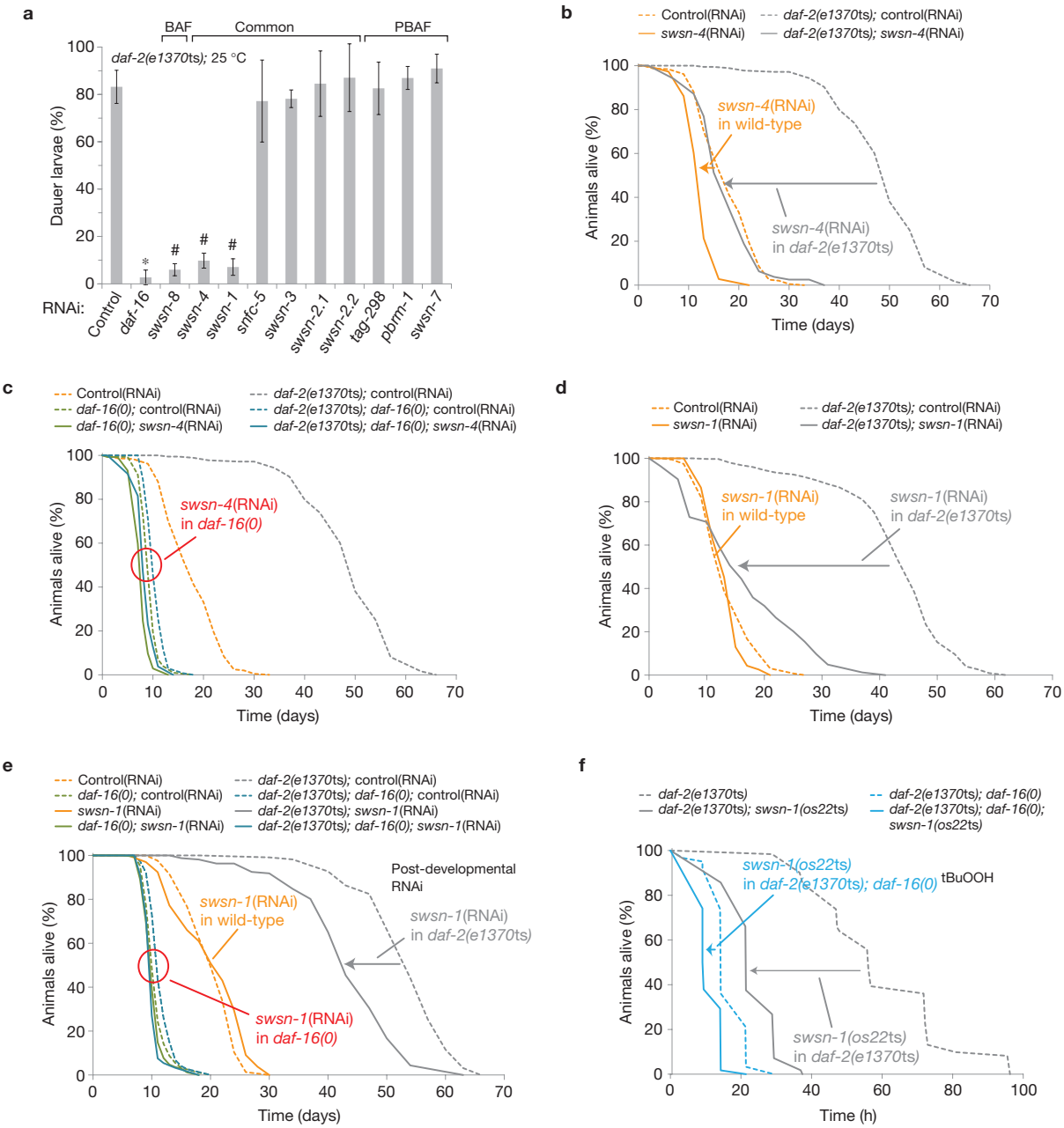

Figure 6 SWI/SNF is required for DAF-16/FOXO-mediated dauer formation, stress resistance and longevity. (**a**) Dauer suppression assay. Eggs of *C. elegans* with activated DAF-16/FOXO (*daf-2(e1370*ts)) were placed on the indicated RNAi bacteria and grown at restrictive temperature. Dauers were identified after 5 days on the basis of morphology and their resistance to 1% SDS. Common SWI/SNF subunits or ones specific to the subclasses BAF or PBAF are indicated accordingly. Marked RNAi clones (*,#) were significantly different from control RNAi (*t*-test; $P < 0.05$), some of which (#) led to non-dauer arrest around the L3 stage. (See Supplementary Fig. S6a; $n = 50$ animals; error bars are based on s.d. from 3 independent experiments.) (**b**–**d**) Lifespan phenotypes caused by inactivation of SWI/SNF. Indicated strains were grown from the L1 stage on the indicated RNAi bacteria. Animals were shifted to restrictive temperature at the L4 stage. (**e**) Post-developmental inactivation of SWI/SNF also impairs DAF-16/FOXO-mediated longevity. Indicated *C. elegans* strains were grown from the L1 stage on *Escherichia coli* HT115. At the L4 stage, animals were shifted to the indicated RNAi bacteria and *e1370*ts was inactivated by a shift to restrictive temperature. (**f**) Oxidative stress resistance assay. Indicated strains were grown to the L4 stage, when *e1370*ts and *os22*ts alleles were inactivated by a shift to restrictive temperature. Twenty-four hours later, animals were exposed to 6 mM tert-butylhydroperoxide (tBuOOH) and their survival was monitored. All survival data of panels (**b**–**f**) were obtained from a minimum of 100 animals per condition, mean survival times and s.e.m. were obtained by Kaplan–Meier analysis, and significant differences between conditions were determined by log-rank test (for exact numbers of animals and statistical data, see Supplementary Table S9).

of *daf-16* but also of several SWI/SNF subunits prevented the formation of SDS-resistant dauer larvae (Fig. 6a). On closer investigation, we found that in the absence of SWI/SNF, animals attempted dauer entry, but full execution of the dauer program failed, leading instead to a DAF-16/FOXO-dependent developmental arrest around the L3 stage (Supplementary Fig. S6a). These arrested animals lacked the typical

longevity of dauer larvae and frequently were void of dauer-specific anatomical features such as the hypodermal alae or the pharyngeal plug (Supplementary Fig. S6b–d). Consistent with our gene expression data (Fig. 2b,d), defective dauer formation was specifically observed on loss of either the core SWI/SNF subunits SWSN-4 and SWSN-1 or the BAF signature subunit SWSN-8, whereas loss of PBAF signature subunits PBRM-1, TAG-298 or SWSN-7 did not disrupt dauer formation. This once again implies a specific role for a BAF-like subclass of SWI/SNF in mediating DAF-16/FOXO functions.

Given this loss-of-function phenotype for SWI/SNF, we also investigated whether overexpression of the SWI/SNF subunits SWSN-4 or SWSN-1 could promote dauer formation. Although gain-of-function phenotypes from such an approach may be difficult to obtain or interpret owing to the multi-subunit nature of the SWI/SNF complex and its requirement to be targeted to the appropriate sites, we observed a *daf-16*-dependent moderate enhancement of dauer formation in *daf-2(e1370*ts) animals at 22 °C (Supplementary Fig. S6e).

SWI/SNF is required for DAF-16/FOXO-mediated longevity and stress resistance

Beyond its role in dauer formation, DAF-16/FOXO is a potent mediator of lifespan extension, in particular during decreased insulin-like signalling. Inactivation of the SWI/SNF core subunits SWSN-4 or SWSN-1 by RNAi fully suppressed this lifespan extension (Fig. 6b,d). Partial suppression was seen on RNAi against the non-core subunit SWSN-3 (Supplementary Fig. S7a). Even post-developmental RNAi against SWI/SNF subunits was sufficient to partially suppress DAF-16/FOXO-induced lifespan extension (Fig. 6e and Supplementary Fig. S7b). All lifespan phenotypes induced by SWI/SNF RNAi were diminished in *daf-16(0)* mutant worms, consistent with SWI/SNF functioning as a cofactor to and thus in the same pathway as DAF-16/FOXO (Fig. 6c,e and Supplementary Fig. S7b). We further confirmed these phenotypes by mutant analysis. Consistent with the RNAi results, the hypomorphic alleles *swsn-4(os13*ts*)* and *swsn-1(os22*ts*)* each impaired DAF-16/FOXO-mediated lifespan extension (Supplementary Fig. S7c,d). Unlike other SWI/SNF alleles or RNAi conditions tested, the particularly strong allele *swsn-1(os22*ts*)* shortened the lifespan of *daf-16(0)* animals, showing that SWI/SNF has some lifespan effects that are independent of DAF-16/FOXO. However, consistent with a requirement of SWI/SNF for DAF-16/FOXO function and thus the two acting in the same pathway, *daf-16(0)* failed to shorten the lifespan of *swsn-1(os22*ts*)* animals (Supplementary Fig. S7d).

The lifespan-extending capabilities of DAF-16/FOXO are highly correlated with its ability to induce stress response pathways[3,24]. We investigated whether SWI/SNF is required for the DAF-16/FOXO-mediated stress resistance of insulin-like signalling mutants. Inactivation of SWI/SNF by *swsn-1(os22*ts*)* or *swsn-3* (RNAi) specifically blocked the enhanced resistance of *daf-2* mutants to oxidative stress (tBuOOH; Fig. 6f and Supplementary Fig. S7e). In addition, *swsn-1(os22*ts*)* was able to block enhanced resistance of *daf-2* mutants to heat stress (32 °C; Supplementary Fig. S7f). Inactivation of SWI/SNF showed a lesser effect in *daf-16* mutant backgrounds (Fig. 6f and Supplementary Fig. S7e,f), again suggesting that SWI/SNF functions in the same pathway as DAF-16/FOXO. Thus, consistent with SWI/SNF being an important cofactor to DAF-16/FOXO, it is not only required for DAF-16/FOXO-mediated gene regulation, but it actually is required for a broad range of DAF-16/FOXO-mediated functions in the animal, in particular dauer formation, stress resistance and the promotion of longevity.

DISCUSSION

Despite our extensive knowledge of pathways leading to DAF-16/FOXO activation, it long remained elusive by which means and the help of which cofactors activated DAF-16/FOXO regulates transcription and thus confers its suite of beneficial effects on the organism. Our study provided the first systematic identification of DAF-16/FOXO cofactors, which in itself provides a significant resource for future studies, and by focusing on its most prominent candidate, the chromatin remodeller SWI/SNF, we were able to illuminate the transcription-regulatory events downstream of DAF-16/FOXO activation. We showed that DAF-16/FOXO is predominantly a transcriptional activator and provided mechanistic insight into how this activation may be achieved—namely by DAF-16/FOXO recruiting a BAF-like subclass of SWI/SNF to target promoters. Extensive exploration of SWI/SNF function in other systems suggests that this recruitment induces local chromatin remodelling to enable binding of downstream transcriptional components and thereby activates transcription[22]. These findings also agree with previous implications of DAF-16/FOXO as a pioneer transcription factor[25,26], suggesting that specifically on pro-longevity stimuli DAF-16/FOXO is activated and autonomously binds to a wide range of target promoters where it nucleates their transcriptional activation by alteration of chromatin states.

Chromatin states and their alteration were previously shown to have profound stress-responsive and lifespan-regulatory effects, but those described alterations were mostly limited to epigenetic changes (in particular histone methylation[27,28] or acetylation[29]) and their mechanistic link to known stress-responsive and lifespan-regulatory pathways often remained unclear. We have now established DAF-16/FOXO-controlled stress-responsive and lifespan-regulatory roles for a type of chromatin alteration fundamentally distinct from epigenetic changes, namely ATP-dependent chromatin remodelling conferred by SWI/SNF. This opens a new dimension to how an alteration of chromatin states can regulate stress response and longevity. Furthermore, any potential cross-talk between this ATP-dependent chromatin remodelling and lifespan-regulatory epigenetic marks will be important to investigate in the future. For example, enrichment of SWI/SNF at DAF-16/FOXO-binding sites is substantially but not entirely dependent on DAF-16/FOXO (Fig. 5b–d and Supplementary Fig. S4) and thus may be supported by other factors or epigenetic marks, with histone acetylation being a strong candidate[30].

Finally, it should be noted that FOXO and SWI/SNF are both evolutionarily conserved and that FOXO also has lifespan regulatory roles in humans[31,32]. Hence, the here described roles of SWI/SNF may be conserved, and their further exploration may eventually benefit our understanding of ageing and age-related diseases in humans. □

METHODS

Methods and any associated references are available in the online version of the paper.

Note: Supplementary Information is available in the online version of the paper

ACKNOWLEDGEMENTS

We thank H. Sawa (National Institute of Genetics, Japan), S. Mitani (Tokyo Women's Medical University, Japan), M. Hansen (Sanford-Burnham Medical Research Institute, USA) and the Caenorhabditis Genetics Center for strains. We thank G. Hayes, U. Kim, M. Borowski, A. Puczinska and D. Grau for experimental support. We thank I. Cheeseman, K. Bouazoune, M. Simon, B. Ardehali, W. Mair, T. Montgomery and the Avruch laboratory for helpful discussions. This work was supported by grants from the National Institutes of Health to G.R. (AG014161 and AG016636), J.M.A. (5P30CA006516 and 2P01CA120964), J.A.W. (F32GM093491), N.V.K. (F32AI100501-01) and R.E.K. (GM048405). C.G.R. was supported by long-term fellowships from the Human Frontier Science Program and the European Molecular Biology Organization, R.H.D. by the American Cancer Society (122240-PF-12-078-01-RMC), N.V.K. by a Tosteson Postdoctoral Fellowship Award, S.K.B. by the Damon Runyon Cancer Research Foundation, and T.H. by the Glenn Foundation for Medical Research and the Austrian Science Fund (FWF).

AUTHOR CONTRIBUTIONS

C.G.R. and G.R. conceived and designed the experiments. C.G.R., G.F.L., N.V.K., J.A.W. and J.M.A. conducted the experiments. R.H.D. analysed the mRNA-seq and ChIP-seq data. S.K.B., R.E.K., T.H. and A.D. provided unpublished methods, materials and advice. C.G.R. and G.R. wrote the manuscript.

COMPETING FINANCIAL INTERESTS

The authors declare no competing financial interests.

Published online at www.nature.com/doifinder/10.1038/ncb2720
Reprints and permissions information is available online at www.nature.com/reprints

1. Kenyon, C. The plasticity of ageing: insights from long-lived mutants. *Cell* **120,** 449–460 (2005).
2. Calnan, D. R. & Brunet, A. The FoxO code. *Oncogene* **27,** 2276–2288 (2008).
3. Murphy, C. T. *et al.* Genes that act downstream of DAF-16 to influence the lifespan of *Caenorhabditis elegans*. *Nature* **424,** 277–283 (2003).
4. Gerstein, M. B. *et al.* Integrative analysis of the *Caenorhabditis elegans* genome by the modENCODE project. *Science* **330,** 1775–1787 (2010).
5. Berdichevsky, A., Viswanathan, M., Horvitz, H. R. & Guarente, L. *C. elegans* SIR-2.1 interacts with 14-3-3 proteins to activate DAF-16 and extend life span. *Cell* **125,** 1165–1177 (2006).
6. Samuelson, A. V, Carr, C. E. & Ruvkun, G. Gene activities that mediate increased life span of *C. elegans* insulin-like signalling mutants. *Genes Dev.* **21,** 2976–2994 (2007).
7. Pollina, E. A. & Brunet, A. Epigenetic regulation of ageing stem cells. *Oncogene* **30,** 3105–3126 (2011).
8. Hartl, F. U., Bracher, A. & Hayer-Hartl, M. Molecular chaperones in protein folding and proteostasis. *Nature* **475,** 324–332 (2011).
9. Margalit, A. *et al.* Barrier to autointegration factor blocks premature cell fusion and maintains adult muscle integrity in *C. elegans*. *J. Cell Biol.* **178,** 661–673 (2007).
10. Curran, S. P. & Ruvkun, G. Lifespan regulation by evolutionarily conserved genes essential for viability. *PLoS Genet.* **3,** e56 (2007).
11. Kwon, C. S. & Wagner, D. Unwinding chromatin for development and growth: a few genes at a time. *Trends Genet.* **23,** 403–412 (2007).
12. Hargreaves, D. C. & Crabtree, G. R. ATP-dependent chromatin remodelling: genetics, genomics and mechanisms. *Cell Res.* **21,** 396–420 (2011).
13. Phelan, M. L., Sif, S., Narlikar, G. J. & Kingston, R. E. Reconstitution of a core chromatin remodelling complex from SWI/SNF subunits. *Mol. Cell* **3,** 247–253 (1999).
14. Moshkin, Y. M., Mohrmann, L., Van Ijcken, W. F. J. & Verrijzer, C. P. Functional differentiation of SWI/SNF remodelers in transcription and cell cycle control. *Mol. Cell. Biol.* **27,** 651–661 (2007).
15. Shibata, Y., Uchida, M., Takeshita, H., Nishiwaki, K. & Sawa, H. Multiple functions of PBRM-1/Polybromo- and LET-526/Osa-containing chromatin remodelling complexes in *C. elegans* development. *Dev. Biol.* **361,** 349–357 (2012).
16. Holstege, F. C. *et al.* Dissecting the regulatory circuitry of a eukaryotic genome. *Cell* **95,** 717–728 (1998).
17. Sawa, H., Kouike, H. & Okano, H. Components of the SWI/SNF complex are required for asymmetric cell division in *C. elegans*. *Mol. Cell* **6,** 617–624 (2000).
18. Libina, N., Berman, J. R. & Kenyon, C. Tissue-specific activities of *C. elegans* DAF-16 in the regulation of lifespan. *Cell* **115,** 489–502 (2003).
19. Henderson, S. T. & Johnson, T. E. daf-16 integrates developmental and environmental inputs to mediate ageing in the nematode Caenorhabditis elegans. *Curr. Biol.* **11,** 1975–1980 (2001).
20. Murphy, C. T., Lee, S-J. & Kenyon, C. Tissue entrainment by feedback regulation of insulin gene expression in the endoderm of *Caenorhabditis elegans*. *Proc. Natl Acad. Sci.* **104,** 19046–19050 (2007).
21. Farkas, G. *et al.* The Trithorax-like gene encodes the Drosophila GAGA factor. *Nature* **371,** 806–808 (1994).
22. Peterson, C. L. & Workman, J. L. Promoter targeting and chromatin remodelling by the SWI/SNF complex. *Curr. Opin. Genet. Dev.* **10,** 187–192 (2000).
23. Fielenbach, N. & Antebi, A. *C. elegans* dauer formation and the molecular basis of plasticity. *Genes Dev.* **22,** 2149–2165 (2008).
24. Lee, S. S., Kennedy, S., Tolonen, A. C. & Ruvkun, G. DAF-16 target genes that control *C. elegans* life-span and metabolism. *Science* **300,** 644–647 (2003).
25. Zaret, K. S. & Carroll, J. S. Pioneer transcription factors: establishing competence for gene expression. *Genes Dev.* **25,** 2227–2241 (2011).
26. Hatta, M. & Cirillo, L. A. Chromatin opening and stable perturbation of core histone: DNA contacts by FoxO1. *J. Biol. Chem.* **282,** 35583–35593 (2007).
27. Greer, E. L. *et al.* Transgenerational epigenetic inheritance of longevity in *Caenorhabditis elegans*. *Nature* **479,** 365–371 (2011).
28. Greer, E. L. *et al.* Members of the H3K4 trimethylation complex regulate lifespan in a germline-dependent manner in *C. elegans*. *Nature* **466,** 383–387 (2010).
29. Longo, V. D. & Kennedy, B. K. Sirtuins in ageing and age-related disease. *Cell* **126,** 257–268 (2006).
30. Chatterjee, N. *et al.* Histone H3 tail acetylation modulates ATP-dependent remodelling through multiple mechanisms. *Nucleic Acids Res.* **39,** 8378–8391 (2011).
31. Flachsbart, F. *et al.* Association of FOXO3A variation with human longevity confirmed in German centenarians. *Proc. Natl Acad. Sci. USA* **106,** 2700–2705 (2009).
32. Willcox, B. J. *et al.* FOXO3A genotype is strongly associated with human longevity. *Proc. Natl Acad. Sci. USA* **105,** 13987–13992 (2008).

DOI: 10.1038/ncb2720

METHODS

C. elegans were grown on *E. coli* OP50 using standard techniques[33].

Strains and alleles. *daf-16(mgDf47)* was referred to as *daf-16(0)* throughout the manuscript. Strains containing Is[*daf-16P::daf-16::GFP*; *rol-6(su1006)*] were all derived from strain TJ356 (ref. 19). For a detailed list of the used strains, see Supplementary Table S10.

RNAi by feeding. *C. elegans* were grown on *E. coli* HT115 containing dsRNA-expressing plasmids from published collections[34–36]. For *swsn-4*, an analogous RNAi clone was generated by use of the following primers: 5′-cgcgaagctcgtgttacc-3′/ 5′-acttcgttgaccttccagtatg-3′. HT115 containing empty plasmid served as a control throughout the manuscript.

Preparation of *C. elegans* lysates for size-exclusion chromatography and immunoprecipitations. *C. elegans* were grown asynchronously at 15 °C, then shifted for 20 h to 25 °C and collected. Animals were washed into lysis buffer (50 mM HEPES at pH 7.4, 1 mM EGTA, 1 mM $MgCl_2$, 150 mM KCl, 10% (v/v) glycerol, Complete (Roche), 1 mM phenylmethyl sulphonyl fluoride and phosphatase inhibitors (Calbiochem)) and lysed by either bead beating or grinding under liquid nitrogen. NP-40 was added to 0.05% (v/v), and the resulting lysate was cleared at 20,000*g*.

Size-exclusion chromatography. Worm lysates were run on a Superose 6 10/300 column (GE Healthcare) in lysis buffer containing 0.05% (v/v) NP-40.

DAF-16/FOXO purification (large scale). *C. elegans* lysate (20 ml) at a protein concentration of 20 mg ml^{-1} was prepared as mentioned above. GFP-tagged DAF-16/FOXO was immunoprecipitated using anti-GFP antibody (3E6, Invitrogen) coupled to Protein A resin (Biorad). Immunoprecipitated proteins were eluted using 100 mM glycine at pH 2.6. As negative controls for background subtraction in Supplementary Table S1, the purification and later mass spectrometry analyses were conducted using wild-type *C. elegans* and *C. elegans* expressing unconjugated GFP from a ubiquitously expressing promoter (strain GR1912).

Mass spectrometry. Samples were digested overnight at pH 8.3 using sequencing-grade trypsin and the resulting peptides separated by micro-capillary reverse-phase chromatography and identified by online tandem mass spectrometry using an LTQ Orbitrap XL hybrid linear ion trap-orbitrap high-resolution mass spectrometer (Thermo). Tandem mass spectra produced by collision induced dissociation (CID) in the ion trap were searched against the Wormpep database (version 221) using ProLuCID (ref. 37) and DTASelect (ref. 38). False discovery rates (FDRs) were determined by searching the mass spectra against the reversed sequences of the Wormpep database. For the data in Supplementary Table S1, proteins had to be identified by a minimum total of two independent peptides across experiments, resulting in an FDR below 1%. Samples were compared using Contrast[38]. Any proteins that were identified also in the control purifications were probably contaminants and thus eliminated from Supplementary Table S1, unless they were identified by at least fivefold higher spectral counts in the combined DAF-16 purifications.

Co-immunoprecipitation. Worm lysates were prepared as mentioned above. FLAG-tagged DAF-16/FOXO was immunoprecipitated using M2 antibody resin (Sigma) and eventually eluted using 250 μg ml^{-1} 3xFLAG peptide. GFP-tagged SWSN-4 was immunoprecipitated using GFP-Trap resin (Chromotek).

Reporter assays. *C. elegans* strains CF1580 or GR1911 were seeded as synchronized L1 onto plates with RNAi bacteria, grown at 15 °C until the L4 stage, and then shifted to 25 °C. Production of progeny was prevented by post-developmental exposure to 5-fluoro-2'-deoxyuridine (FUDR; ref. 39). GFP expression was analysed on day 4 of adulthood, using Zeiss Discovery V12 and Zeiss Axio Imager fluorescence microscopes.

mRNA isolation, reverse transcription and qPCR. Animals were seeded by egg-lay onto plates with OP50 bacteria, grown at 15 °C until the L4 stage, and then shifted for 20 h to 25 °C. Animals were collected and total RNA extracted using Trizol. mRNA quantification by reverse transcription and qPCR was performed as previously described[40]. Samples were normalized to *Y45F10D.4* transcript levels[41]. Experiments were conducted in biological duplicate. Primers used were previously published[41,42] or as follows: *ins-7* 5′-GCATGCGAATCGAATACTGA-3′/5′-GAAGTCGTCGGTGCATTCTT-3′, *hsp-12.6* 5′-GGAGATGGAGTTGTCAATGTCCT-3′/ 5′-TCCTTCTTTACATTGT-GCTCCA-3′.

ChIP–qPCR. Animals were grown asynchronously at 15 °C and then shifted for 20 h to 25 °C. ChIP was performed in biological duplicate as previously described[40]. Primers used for qPCR were: *hil-1P* 5′-ACAATTCGTTCGTCGGTCTC-3′/ 5′-AGGACGGGCCTCTTCTATTC-3′, *ctl-3P* 5′-TATAAAAGAGGCGGCCAGAC-3′/ 5′-CCTTCTCAGCGAGCAGTTCT-3′, control (Supplementary Fig. S4b, left panel) 5′-CTCTTCATTTTGTTCCTGTGTTTTCC-3′/ 5′-GAAGGCGGCGGTAATTGT-TG-3′, control (Supplementary Fig. S4b, middle and right panel) 5′-AC-TGGGAGTGGTTCAAGTGG-3′/5′-TACCTCCAGCACCACCTTCT-3′. Primers for *sod-3P* were published previously[42].

Construction of sequencing libraries. mRNA-seq libraries were constructed using a TrueSeq RNA SamplePrep V2 kit (Illumina). For construction of ChIP-seq libraries, DNA was end-repaired, A-tailed, ligated to universal adapters, and amplified for 12 cycles with indexed primers modified according to ref. 43. Excess adapters were removed by purification with AMPure XP magnetic beads (Beckman Coulter).

High-throughput sequencing. Multiplexed single-end ChIP-seq and mRNA-seq libraries were sequenced for 50 cycles using either Illumina HiSeq 2000 or Illumina MiSeq according to the manufacturer's instructions. Image analysis, base calling and quality scoring were performed in real time with the standard Illumina analysis pipeline using a phiX control.

Processing of mRNA-seq reads and differential expression analysis. Reads were aligned to the *C. elegans* genome with the TopHat (v2.0.4) software package[44] using known gene model annotations (WS220). Transcript abundance (FPKM, fragments per kilobase of transcript per million fragments) and differential expression were calculated using Cuffdiff (v2.0.2) included in the Cufflinks software package[45] using the following parameters: -m 160 -s 40 -u –upper-quartile-norm –compatible-hits-norm –library-type fr-unstranded. All conditions/samples were analysed in biological duplicate. Statistically significant differentially expressed genes (DEGs) were identified using a 5% FDR. Differential gene expression values were calculated as the ratio of FPKM values. To test for significant overlap between gene lists (Fig. 3c) the hypergeometric test was used (*phyper* R function).

To determine the function of SWSN-1 at DAF-16-regulated genes (Fig. 3d), all protein-coding genes were classified as DAF-16 activated, repressed or unregulated (Cuffdiff, 5% FDR) and differential gene expression values were calculated (relative to *daf-2(e1370*ts) control). Unexpressed genes having a FPKM of 0 in any of the samples were removed from analysis. Genes were ordered from least to most mis-expressed in *daf-2(e1370*ts); *daf-16(0)* for each class of genes and the corresponding differential expression level in *daf-2(e1370*ts); *swsn-1(os22*ts*)* was plotted. Finally, a smoothed line representation of the data was plotted using cubic splines (smooth.spline R function, spar = 0.6).

ChIP-seq read processing, peak calling and metagene analysis. Reads were aligned to the *C. elegans* genome (WS220) using Bowtie (v0.12.8) with the following parameters: -m 1 –best –strata[46]. Uniquely mapping reads containing no more than one mismatch were used for peak calling and read density calculations. Enriched peaks were identified using MACS (v1.4.0) with the following parameters: –mfold = 5,30 –bw = 175 –keep-dup = auto[47]. Statistically significant peaks ($P < 1\times10^{-5}$) were filtered using a 1% FDR. Genomic regions that are commonly identified in ChIP-seq experiments, so-called hotspots, represent potential artefacts and were removed from the peak data set as previously described[48]. Data were generated from one of two biological replicates whose reproducibility had been confirmed by ChIP–qPCR at various loci (Supplementary Fig. S4b).

To calculate genome-wide read densities, reads were first extended to mean fragment size (175 base pairs (bp)) in the 3′ direction of the read to more precisely reflect the true binding position. Next, the number of reads within 25-bp non-overlapping bins was determined across the genome and each read count was normalized by the library size. This procedure was performed for both immunoprecipitation and input ChIP samples. The input read count was then subtracted from the immunoprecipitation count for every bin. To compare DAF-16::GFP, SWSN-4::GFP or SWSN-1::GFP binding at DAF-16 peaks (Figs 4c–e, 5a–c and Supplementary Fig. S3a), the normalized genome-wide read counts for the two samples were first quantile-normalized using the preprocessCore R package[49]. The bin overlapping each DAF-16 peak summit (MACS) was identified and the mean normalized read count was calculated for each sample. This process was repeated for 40 bins upstream and 40 bins downstream of the peak summit (±1,000 bp). Data smoothing was performed before plotting the data with cubic splines (*smooth.spline* R function, *spar* = 0.5). For *P*-value calculations in Fig. 5a,b, indicating whether DAF-16 or SWSN-4 binding had significantly changed between the compared samples, we first determined for each sample the sum of all reads in each of the 81 bins surrounding the DAF-16 peak summits (see

above). The resulting 81 data points were then compared between samples by a t-test[50].

Overlap between sets of binding sites was determined using intersectBED of the BEDTools Utility suite[51] (Fig. 4d).

Associating ChIP-seq peaks with proximal genes. First, the distance between each peak summit (MACS) and nearby transcriptional start sites (TSS) of protein-coding genes was calculated. A peak summit positioned within 2.5 kb upstream or 300 bp downstream of a TSS was assigned to that gene. If multiple genes could be assigned to a single peak, the closest TSS was selected. If no TSS was found in this window, the peak was left unassigned. Using this approach, genes could be assigned to ~70% of the ChIP-seq peaks (bound genes). The distribution of peak to TSS distances is plotted in Fig. 4a, which also includes long-range distances that fall outside the −2.5 kb to +300 bp window. Finally, enrichment of differential gene expression for bound genes (Fig. 4b) was calculated as (number of bound DEGs/ number of bound expressed genes) / (number of DEGs/ number of expressed genes), where expressed genes are defined as genes where FPKM > 0 in the *daf-2(e1370*ts) and *daf-2(e1370*ts); *daf-16(0)* samples.

Identification of DNA motifs enriched at DAF-16/FOXO- and SWI/SNF-binding sites. Binding sites obtained from ChIP-seq analysis were searched for enriched DNA motifs using peak motifs at http://rsat.ulb.ac.be. Searches were conducted using default parameters and an oligomer length of 7. Significance scores were determined as previously described[52].

Dauer assays. *C. elegans* strains CB1370, GR1309, GR1900 or GR1908 were seeded by egg-lay onto RNAi bacteria and grown at 25 °C. Animals were evaluated after 5 days, either by scoring their dauer morphology or their survival of a 30 min treatment with 1% (w/v) SDS (ref. 53).

Lifespan assays of gene inactivations by RNAi. *C. elegans* strains GR1373, GR1899, GR1901 or AU119 were seeded as synchronized L1 onto RNAi bacteria, grown at 15 °C until the L4 stage, and then shifted to 20 °C. Production of progeny was prevented by post-developmental exposure to FUDR (ref. 39). Survival of animals was assayed every 2 days, as described previously[39]. Gene inactivation by post-developmental RNAi and the large-scale screening of Supplementary Tables S2 and S4 were conducted as previously described[6,10].

Lifespan assays of mutants. Animals were seeded by egg-lay onto OP50 bacteria, grown at 15 °C until the L4 stage, and then shifted to 25 °C. Production of progeny was prevented by post-developmental exposure to FUDR (ref. 39). Survival of animals was assayed every 2 days, as described previously[39].

Stress assays. For oxidative stress under RNAi, animals were seeded by egg-lay onto plates with RNAi bacteria, grown at 15 °C until the L4 stage, and then shifted to 20 °C. From day 1 of adulthood, animals were exposed to 6 mM tert-butylhydroperoxide (tBuOOH) and their survival was scored, as previously described[54]. For stress assays of mutant animals, animals were seeded by egg-lay onto plates with OP50 bacteria, grown at 15 °C until the L4 stage, and then shifted to 25 °C. From day 1 of adulthood, animals were exposed to 6 mM tBuOOH (oxidative stress) or shifted to 32 °C (heat stress) and their survival was scored, as previously described[54].

Microscopy. Live animals were analysed at ×65 magnification using a Zeiss Discovery V12 microscope. For imaging, worms were paralysed with 2,3-butanedione monoxime, mounted on agarose pads, and imaged on a Zeiss Axio Imager at magnifications of ×100, ×400 or ×630.

Statistical analysis. Lifespan and stress resistance assays were evaluated by Kaplan–Maier and log-rank tests; dauer formation, qPCR and analyses of Supplementary Figs S2, S6b,e were evaluated by Student's t-test. P values of Fig. 4b were determined by hypergeometric test. Statistical tests for other experiments are stated in the respective methods sections, tables or figure legends. Analyses were performed using either Winstat (R. Fitch Software), Origin (Originlab) or R (ref. 55).

High-throughput sequencing and mass spectrometry raw data. Primary accessions: SRP017908 and SRP017927 at the Sequence Read Archive (SRA) at NCBI. PASS00130 at PeptideAtlas. Referenced accessions: GSE15567 at the Gene Expression Omnibus (GEO) at NCBI provides the DAF-16 ChIP-seq data of the modENCODE consortium.

33. Stiernagle, T. Maintenance of *C. elegans*. *WormBook* 1–11 (2006).
34. Ahringer, J. Reverse genetics. *WormBook* 1–43 (2006).
35. Rual, J. F. *et al*. Toward improving *Caenorhabditis elegans* phenome mapping with an ORFeome-based RNAi library. *Genome Res.* **14,** 2162–2168 (2004).
36. Kamath, R. S. *et al*. Systematic functional analysis of the *Caenorhabditis elegans* genome using RNAi. *Nature* **421,** 231–237 (2003).
37. Xu, T. *et al*. ProLuCID, a fast and sensitive tandem mass spectra-based protein identification program. *Mol. Cell. Proteomics* **5,** S174 (2006).
38. Tabb, D. L., McDonald, W. H. & Yates, J. R. DTASelect and Contrast: tools for assembling and comparing protein identifications from shotgun proteomics. *J. Proteome Res.* **1,** 21–26 (2002).
39. Hamilton, B. *et al*. A systematic RNAi screen for longevity genes in *C. elegans*. *Genes Dev.* **19,** 1544–1555 (2005).
40. Curran, S. P., Wu, X., Riedel, C. G. & Ruvkun, G. A soma-to-germline transformation in long-lived *Caenorhabditis elegans* mutants. *Nature* **459,** 1079–1084 (2009).
41. Hoogewijs, D., Houthoofd, K., Matthijssens, F., Vandesompele, J. & Vanfleteren, J. R. Selection and validation of a set of reliable reference genes for quantitative sod gene expression analysis in *C. elegans*. *BMC Mol. Biol.* **9,** 9 (2008).
42. Li, J. *et al*. *Caenorhabditis elegans* HCF-1 functions in longevity maintenance as a DAF-16 regulator. *PLoS Biol.* **6,** e233 (2008).
43. Bentley, D. R. *et al*. Accurate whole human genome sequencing using reversible terminator chemistry. *Nature* **456,** 53–59 (2008).
44. Trapnell, C., Pachter, L. & Salzberg, S. L. TopHat: discovering splice junctions with RNA-Seq. *Bioinformatics* **25,** 1105–1111 (2009).
45. Trapnell, C. *et al*. Transcript assembly and quantification by RNA-Seq reveals unannotated transcripts and isoform switching during cell differentiation. *Nat. Biotechnol.* **28,** 511–515 (2010).
46. Langmead, B., Trapnell, C., Pop, M. & Salzberg, S. L. Ultrafast and memory-efficient alignment of short DNA sequences to the human genome. *Genome Biol.* **10,** R25 (2009).
47. Zhang, Y. *et al*. Model-based analysis of ChIP-Seq (MACS). *Genome Biol.* **9,** R137 (2008).
48. Niu, W. *et al*. Diverse transcription factor binding features revealed by genome-wide ChIP-seq in *C. elegans*. *Genome Res.* **21,** 245–254 (2011).
49. Bolstad, B. M., Irizarry, R. a, Astrand, M. & Speed, T. P. A comparison of normalization methods for high density oligonucleotide array data based on variance and bias. *Bioinformatics* **19,** 185–193 (2003).
50. Whyte, W. a *et al*. Enhancer decommissioning by LSD1 during embryonic stem cell differentiation. *Nature* **482,** 221–225 (2012).
51. Quinlan, A. R. & Hall, I. M. BEDTools: a flexible suite of utilities for comparing genomic features. *Bioinformatics* **26,** 841–842 (2010).
52. Thomas-Chollier, M. *et al*. A complete workflow for the analysis of full-size ChIP-seq (and similar) data sets using peak-motifs. *Nat. Protoc.* **7,** 1551–1568 (2012).
53. Cassada, R. C. & Russell, R. L. The dauer larva, a post-embryonic developmental variant of the nematode *Caenorhabditis elegans*. *Dev. Biol.* **46,** 326–342 (1975).
54. Rizki, G. *et al*. The evolutionarily conserved longevity determinants HCF-1 and SIR-2.1/SIRT1 collaborate to regulate DAF-16/FOXO. *PLoS Genet.* **7,** e1002235 (2011).
55. R Development Core Team R: A language and environment for statistical computing. (2010). at http://www.r-project.org/.

nature cell biology

DOI: 10.1038/ncb2720

a

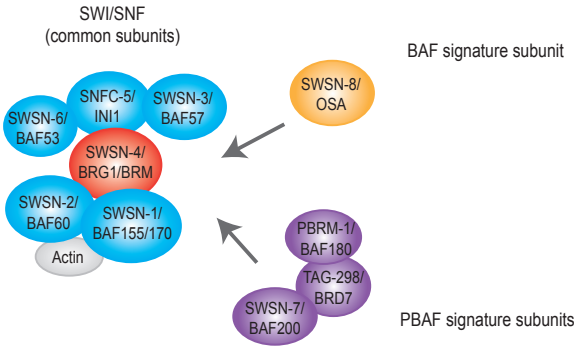

b

C. elegans protein name	public name	MW [kDa]	annotation	yeast ortholog	fly ortholog	human ortholog
F01G4.1	SWSN-4	170.6	catalytic subunit	Swi2/Snf2, Sth1	Brahma	BRG1/hBRM
Y113G7B.23	SWSN-1	85.4	core subunit	Swi3	Moira	BAF155, BAF170
R07E5.3	SNFC-5	42.8	core subunit, not essential in *C. elegans*	Snf5	SNR1	hSNF5/INI1
ZK1128.5/C18E3.2	SWSN-2.1/2.2	51.7/52.2	accessory subunit	Rsc6, Swp73	BAP60	BAF60
Y71H2AM.17	SWSN-3	38.9	accessory subunit	--	BAP111	BAF57
ZK616.4	SWSN-6	48.4	accessory subunit	Arp7, Arp9	BAP55	BAF53
C01G8.9	SWSN-8*	181.2	signature subunit, BAF subclass specific	Swi1	OSA	hOSA/BAF250
C26C6.1	PBRM-1*	216.6	signature subunit, PBAF subclass specific	Rsc1, Rsc2, Rsc4	Polybromo	BAF180
C08B11.3	SWSN-7*	139.1	signature subunit, PBAF subclass specific	Rsc9	BAP170	BAF200
C01H6.7	TAG-298*	71.3	signature subunit, PBAF subclass specifc	--	--	BRD7
	actin	~42	monomeric (β-)actin	--	β-actin	β-actin

*: signature subunits

c

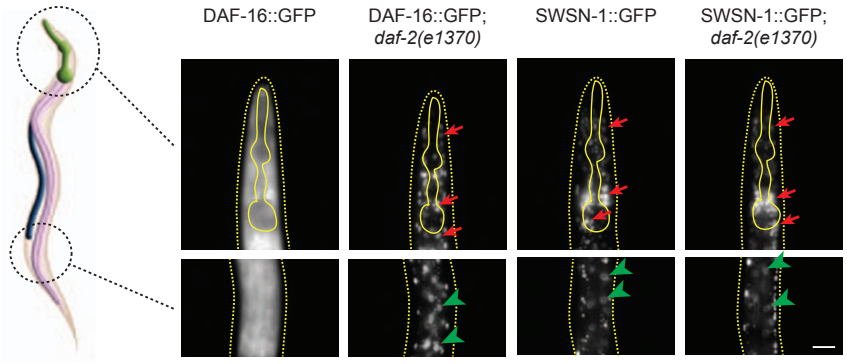

Figure S1 (**a**) The *C. elegans* SWI/SNF complex. Two putative subclasses, analogous to mammalian BAF and PBAF, are distinguished by their association with exclusive signature subunits. Subunits investigated during this study are coloured, with the catalytic subunit depicted in red and signature subunits depicted in orange or purple. (**b**) List of the various predicted *C. elegans* SWI/SNF subunits and their orthologs in yeast, fly and human. Adapted from[11,12,15]. (**c**) Expression/Localization of DAF-16/FOXO and SWI/SNF. *C. elegans* of the indicated genotypes were grown asynchronously. *e1370ts* was inactivated by a shift for 20 h to restrictive temperature. GFP signal in L3 larvae is shown. Yellow lines indicate positions of the cuticle and pharynx. Red arrows indicate sample neuronal nuclei. Green arrowheads indicate sample intestinal nuclei. (scale bar: 20 μm) (The anatomical sketch was adapted from wormbase.org.)

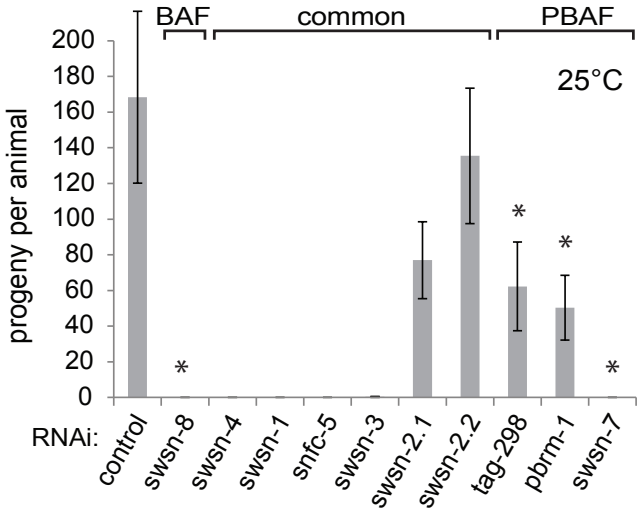

Figure S2 Validation of RNAi conditions for the various SWI/SNF signature subunits. Mostly independent from its involvement with DAF-16/FOXO, loss of either the BAF or PBAF SWI/SNF subclasses leads to defects in germline development[15], which results in reduced brood-size. We used this phenotype to validate the efficiency of our SWI/SNF subunit RNAi conditions. In parallel to the experiments from Figure 2b,d, wild-type *C. elegans* were seeded as L1 onto the indicated RNAi bacteria and grown at 25°C. Progeny for individual animals between days 1 and 3 of adulthood was counted (n=22 animals; error bars based on S.D. between animals). RNAi for all the BAF and PBAF signature subunits yielded significantly reduced brood sizes compared to control conditions (*; t-Test; $p<0.05$), suggesting that those RNAi conditions worked reasonably well.

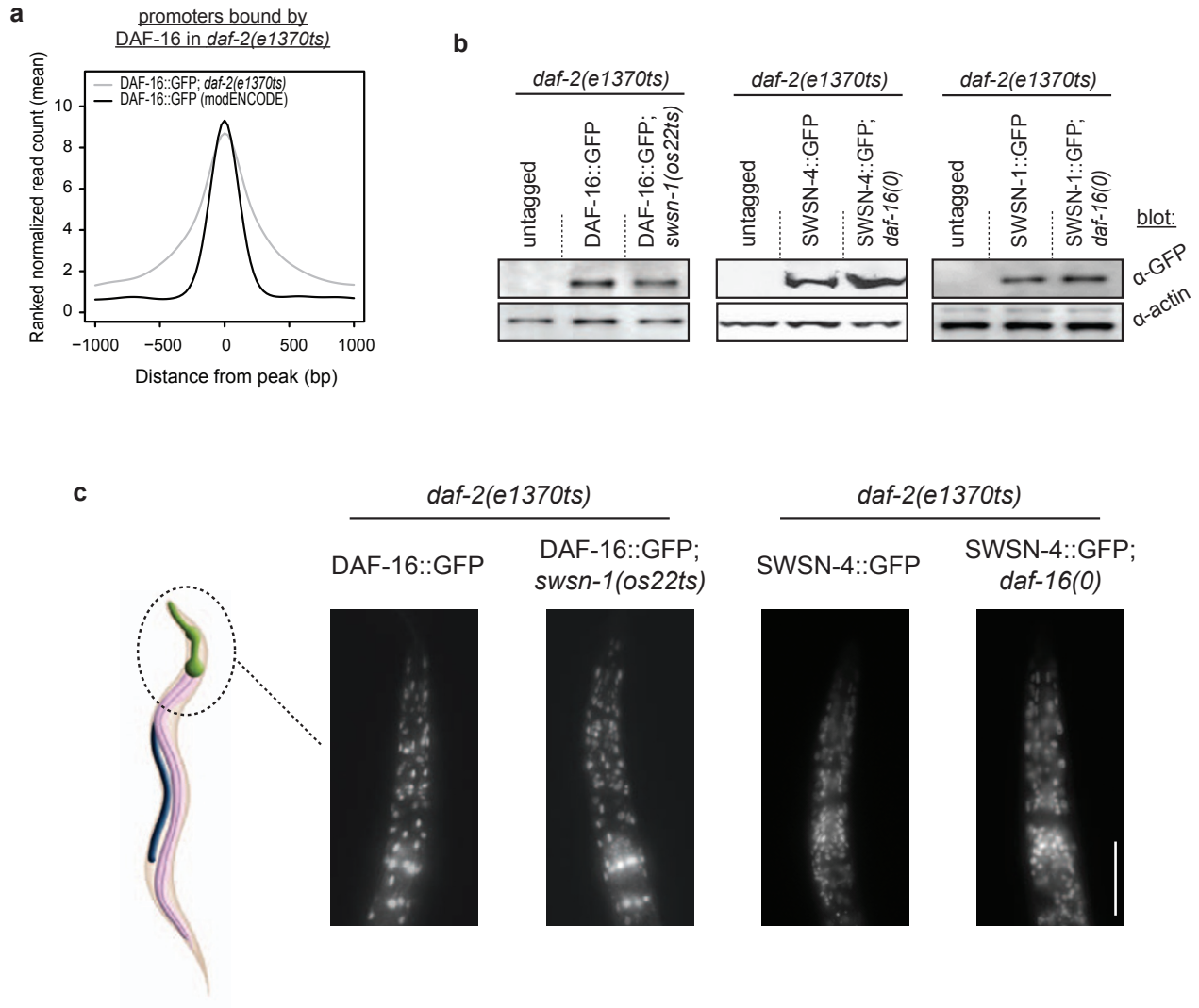

Figure S3 (**a**) Good correlation of our DAF-16/FOXO ChIP-Seq dataset from *daf-2(e1370ts)* with a previous dataset from wild-type animals. Our ChIP-Seq data for DAF-16/FOXO::GFP; *daf-2(e1370ts)* from Figure 4 was compared to data for DAF-16/FOXO::GFP from wild-type animals, previously made available by the modENCODE consortium[4]. Mean read distributions from the two datasets across our DAF-16/FOXO binding sites are shown. (**b**,**c**) DAF-16/FOXO and SWI/SNF do not affect each other's expression levels or nuclear localization. *C. elegans* were grown asynchronously; *e1370ts* and *os22ts* alleles were inactivated by a 20h shift to restrictive temperature. (**b**) Whole worm lysates of indicated strains were analysed by SDS-PAGE and western blotting. (**c**) GFP signal in L4/YA animals of indicated strains is shown. SWSN-1::GFP showed results identical to SWSN-4::GFP (data not shown). (scale bar: 100 μm) (The anatomical sketch was adapted from wormbase.org.)

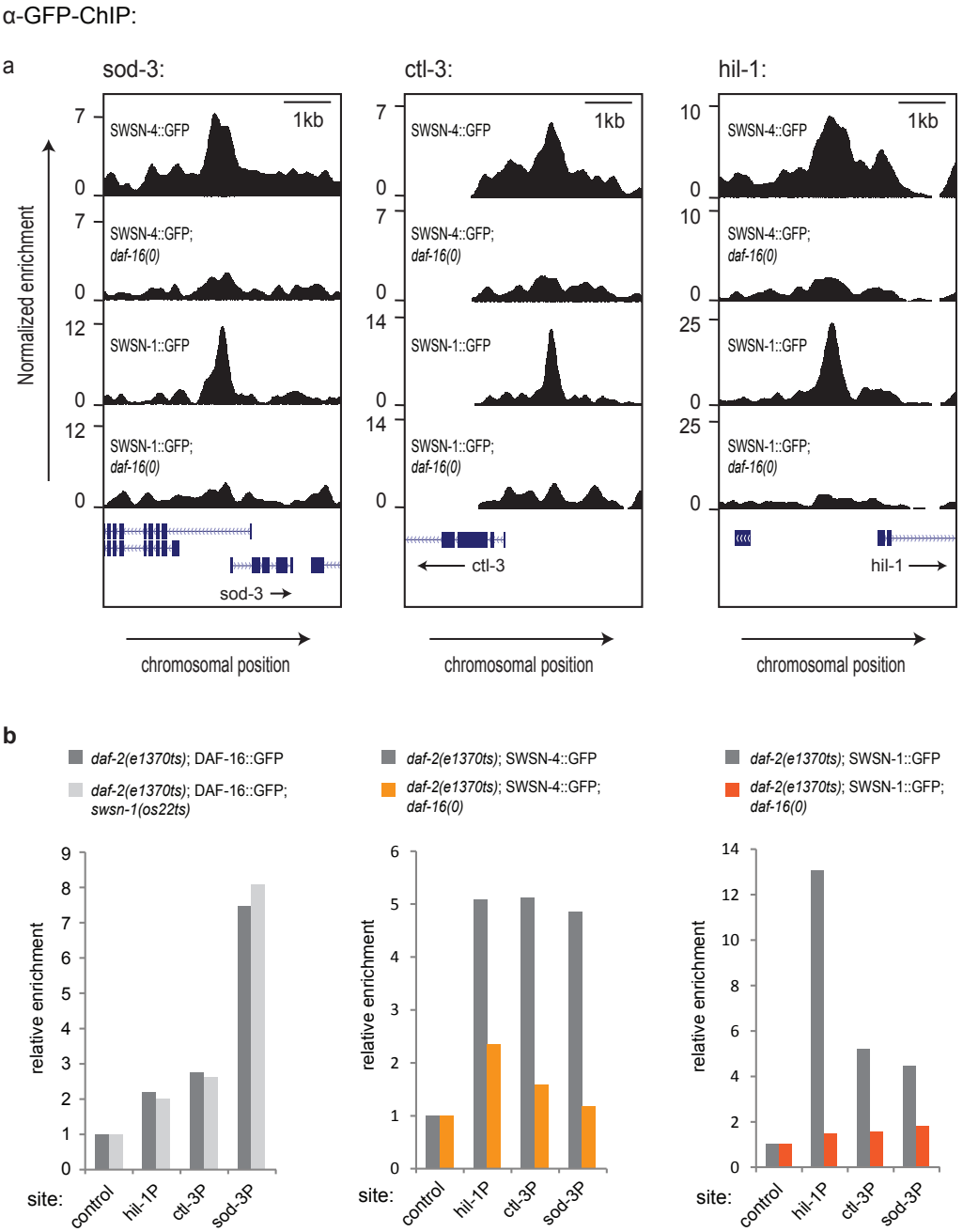

Figure S4 (**a**) *daf-16(0)*-dependent changes in SWI/SNF binding at prominent promoter regions that are directly bound and activated by DAF-16/FOXO. SWSN-4::GFP and SWSN-1::GFP ChIP-Seq data from Figures 5b and 5c was normalized, smoothed over 50 bp bins, and displayed in the UCSC genome browser. *sod-3*, *ctl-3*, and *hil-1* promoter regions are shown. (**b**) Confirmation of the ChIP-Seq data for *sod-3*, *ctl-3*, and *hil-1* promoter regions by conventional ChIP-qPCR.

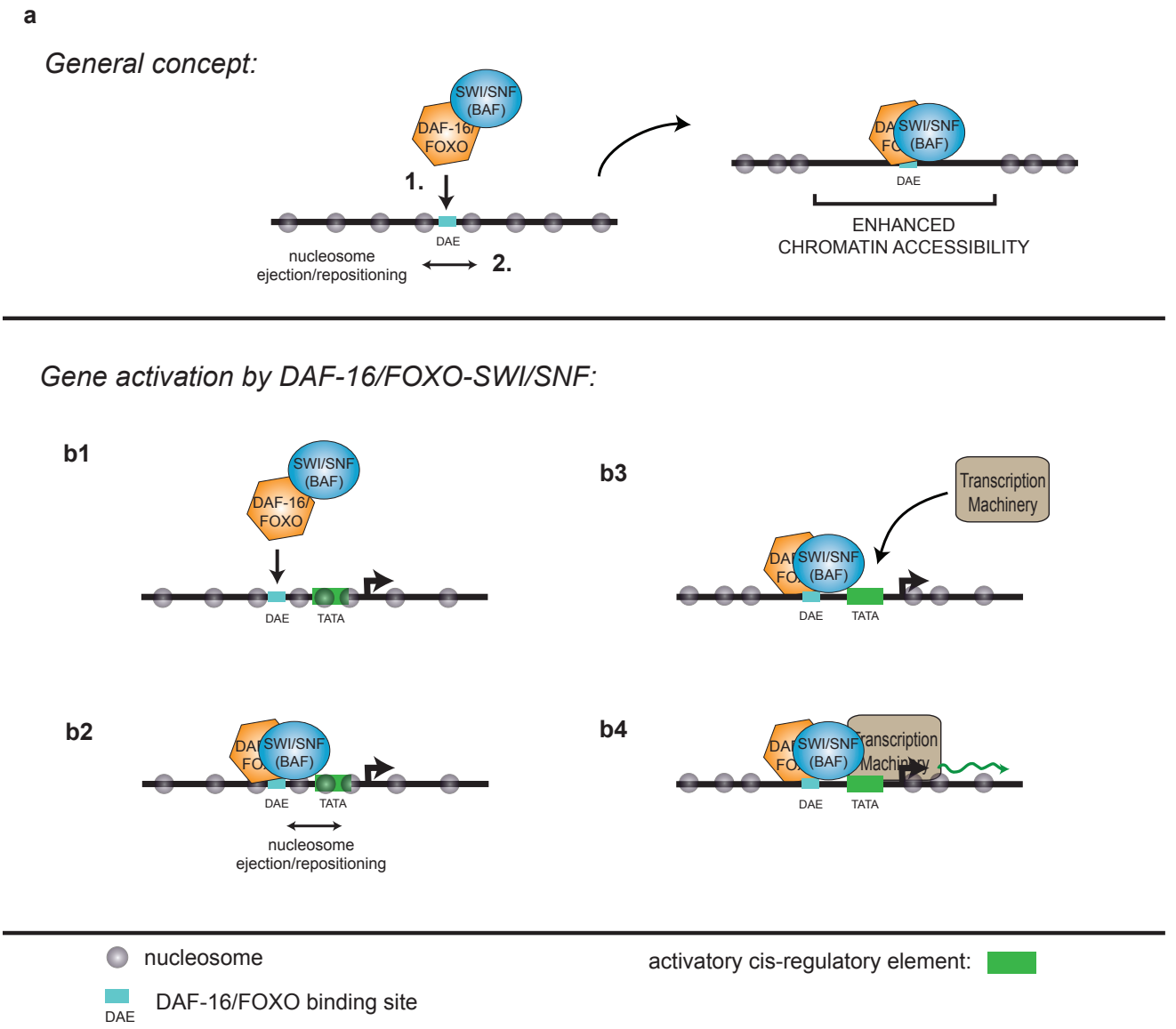

Figure S5 Model for target gene activation by DAF-16/FOXO and SWI/SNF. (**a**) General concept of SWI/SNF recruitment creating a zone of low nucleosome occupancy. This zone allows for better accessibility of contained cis-regulatory elements for binding by downstream components. (**b**) Activation of a target gene by DAF-16/FOXO-SWI/SNF, using the example of a DAF-16/FOXO binding site in proximity to an activatory cis-regulatory promoter element, the TATA box. (**b1**) DAF-16/FOXO binds to its binding site and recruits SWI/SNF(BAF) to this location. (**b2**) Chromatin remodelling by SWI/SNF(BAF) creates a zone of low nucleosome occupancy. (**b3**) The TATA-box is now accessible for binding by the transcription machinery. (**b4**) Transcription is induced. This model is consistent with previously described roles of SWI/SNF as a transcriptional regulatory cofactor[22].

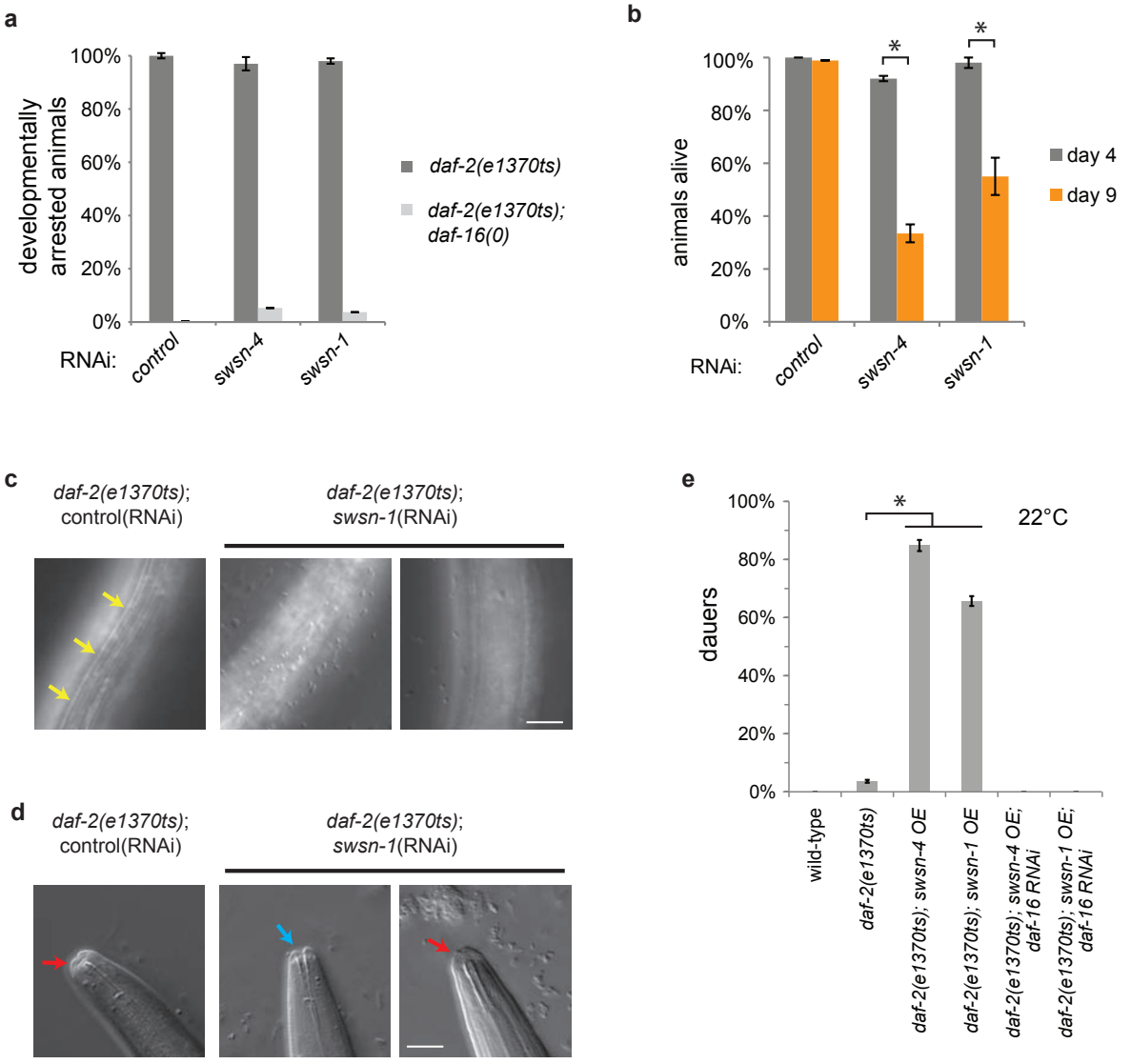

Figure S6 Regulation of dauer formation by SWI/SNF. In *daf-2* mutants, absence of SWI/SNF still allows for DAF-16/FOXO-dependent developmental arrest around the L3 stage (**a**), but those arrested worms lack typical dauer features (**b-d**). (**a**) In parrallel to the experiments from Fig. 6a, indicated *C. elegans* strains were seeded onto the indicated RNAi bacteria and grown at 25°C. 5 days after seeding, animals that had only reached mid to late larval stages were considered developmentally arrested. (n=50; error bars based on S.D. from 3 independent experiments) (**b**-**d**) Eggs of *daf-2(e1370ts)* animals were seeded onto the indicated RNAi bacteria and grown at 25°C. (**b**) Loss of SWI/SNF impairs the longevity of these animals, as indicated by their reduced survival 9 days after seeding. Significant reductions are indicated (*; t-Test; $p<0.05$). (n=50; error bars based on S.D. from 3 independent experiments) (**c**,**d**) 5 days after seeding, *swsn-1* (RNAi) causes common absence of dauer-specific alae (**c**; yellow arrows) and occasional absence of the pharyngeal plug (**d**; red arrows indicate a closed, blue arrows an open pharynx) (scale bars: 10 µm). (**e**) Overexpression of SWSN-4/BRG1 or SWSN-1/BAF155/170 moderately promotes dauer formation in a *daf-16*-dependent manner. Eggs of wild-type, *daf-2(e1370ts)*, *daf-2(e1370ts); SWSN4::GFP OE* (GR1908), or *daf-2(e1370ts); SWSN1::GFP OE* (GR1900) animals were placed on either control or *daf-16* RNAi bacteria and grown at 22°C. Dauers were identified after 5 days based on morphology. Significant enhancements in dauer formation compared to *daf-2(e1370ts)* are indicated (*; t-Test; $p<0.05$). (n=50; error bars based on S.D. from 3 independent experiments).

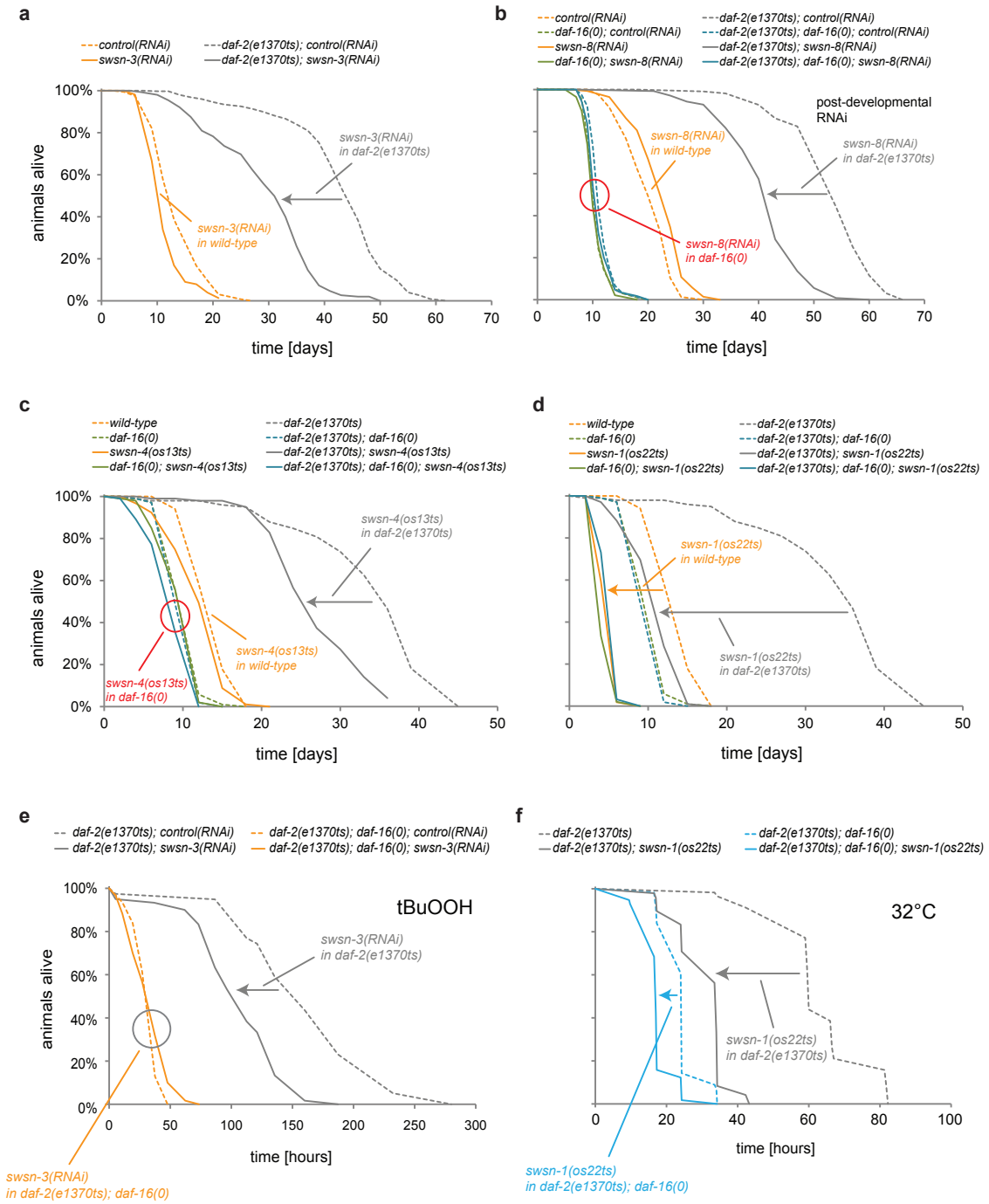

Figure S7 (**a**-**d**) Lifespan phenotypes caused by loss of SWI/SNF subunits. (**a**) Indicated *C. elegans* strains were grown from the L1-stage on the indicated RNAi bacteria. *e1370ts* was inactivated by a shift to restrictive temperature at the L4-stage. (**b**) Post-developmental RNAi. Indicated *C. elegans* strains were grown from the L1-stage on *E. coli* HT115. At the L4-stage, animals were shifted to the indicated RNAi bacteria and *e1370ts* was inactivated by shift to restrictive temperature. (**c**,**d**) Lifespan analyses of SWI/SNF mutant alleles. Indicated *C. elegans* strains were grown at permissive temperature until the L4-stage and then shifted to restrictive temperature, in order to inactivate the *e1370ts*, *os13ts*, and *os22ts* alleles. (**e**,**f**) Stress resistance phenotypes caused by loss of SWI/SNF subunits. Animals were grown from the L1-stage on *E. coli* OP50 or the indicated RNAi bacteria. At the L4-stage, *e1370ts* and *os22ts* alleles were inactivated by shift to restrictive temperature. (**e**) Oxidative stress resistance assay. At day 1 of adulthood, animals were transferred to plates containing 6 mM t-Butylhydroperoxide (tBuOOH) and their survival was monitored. (**f**) Heat stress resistance assay. At day 1 of adulthood, animals were shifted to 32°C and their survival was monitored. All survival data (panels (**a**-**f**)) was obtained from a minimum of 100 animals per condition, mean survival times and S.E.M. were obtained by Kaplan-Meier analysis, and significant differences between conditions were determined by log-rank test (for exact numbers of animals and statistical data see Table S9).

Fig. 1a

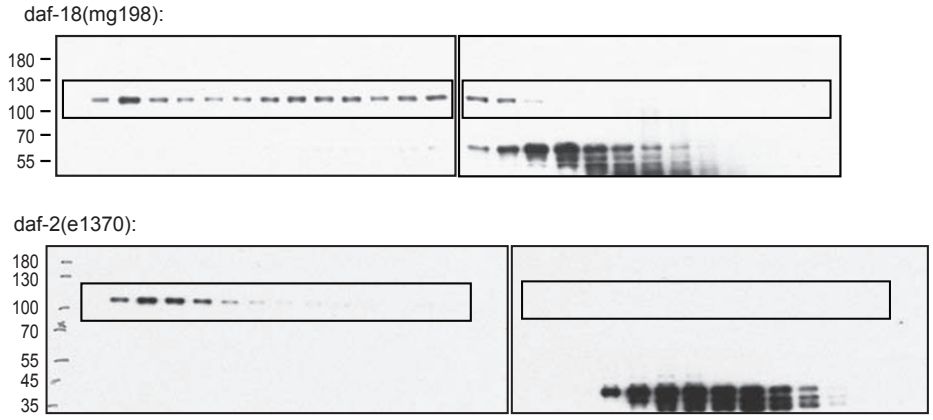

Fig. 1b

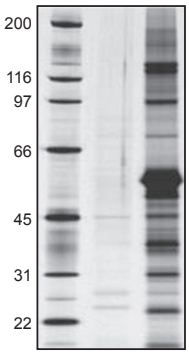

Fig. 1c

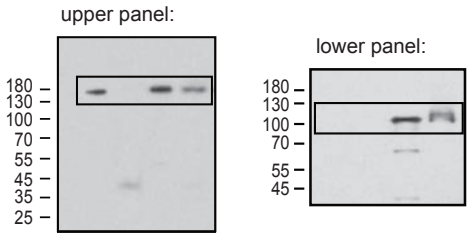

Fig. 1d

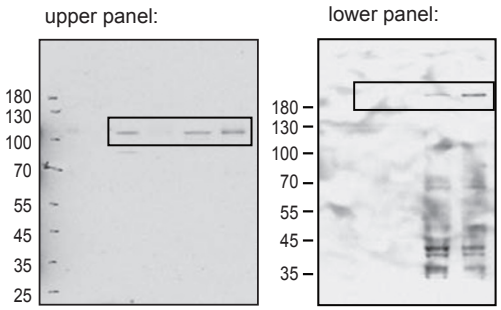

Figure S7 Uncropped key electrophoresis data.